Lawrence Berkeley National Laboratory

Title
Quasi-static analysis of elastic behavior for some systems having higher fracture densities.

Permalink
https://escholarship.org/uc/item/7vn1c9fx

Author
Berryman, J.G.

Publication Date
2010-07-07

Peer reviewed

Quasi-static analysis of elastic behavior for some systems having higher fracture densities

James G. Berryman[1] and Atilla Aydin[2]

[1]Lawrence Berkeley National Laboratory, Earth Sciences Division, One Cyclotron Road MS-90R1116, Berkeley, CA 94720, USA
[2]Department of Geological and Environmental Sciences, Stanford University, Stanford, CA 94305-2115, USA

SUMMARY

Elastic behavior of geomechanical systems with interacting (but not intersecting) fractures are treated using generalizations of the Backus and the Schoenberg-Muir methods for analyzing layered systems whose layers are intrinsically anisotropic due to locally aligned fractures. By permitting the axis of symmetry of the locally anisotropic compliance matrix for individual layers to differ from that of the layering direction, we derive analytical formulas for interacting fractured regions with arbitrary orientations to each other. This procedure provides a systematic tool for studying how contiguous, but not yet intersecting, fractured domains interact, and provides a direct (though approximate) means of predicting when and how such interactions lead to more dramatic weakening effects and ultimately to failure of these complicated systems. The method permits decomposition of the system elastic behavior into specific eigenmodes that can all be analyzed, and provide a better understanding about which of these specific modes are expected to be most important to the evolving failure process.

KEY WORDS: joints, fractures, effective medium theory

1. INTRODUCTION

Natural fractures in geological systems have important consequences for the geomechanical and seismic properties of rocks and reservoirs, as well as for the fluid flow through these fractured rock masses. Once rocks become highly fractured, it is often desirable to measure or estimate their effective properties for various scientific and/or engineering purposes. One reason for this
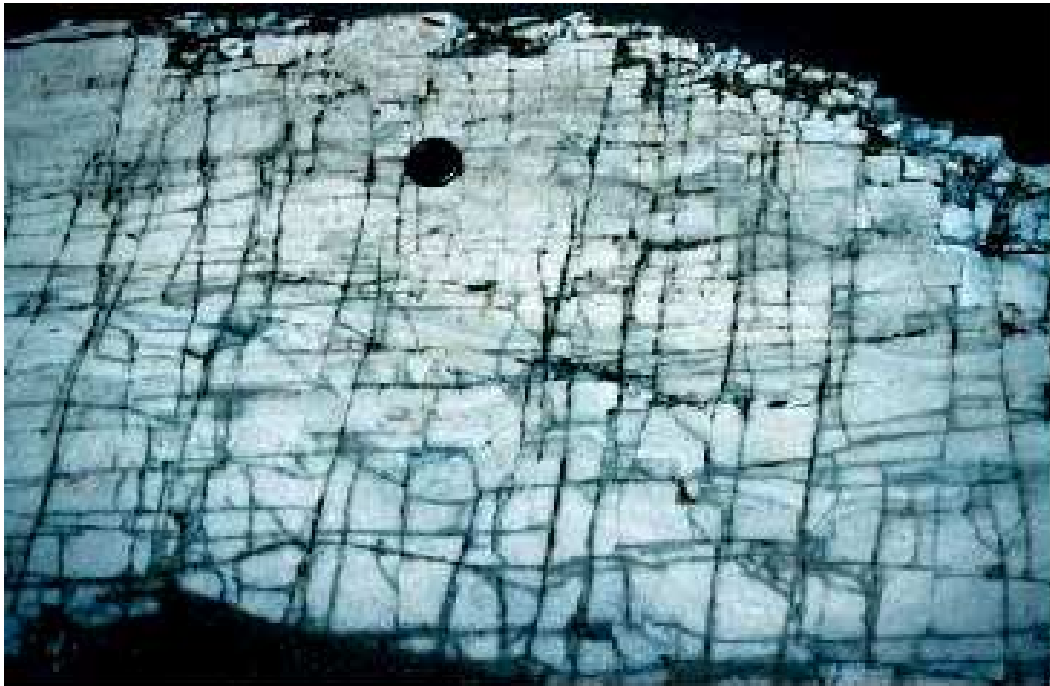
Figure 1. Field example of a fracture network having 90° intersection angles, commonly referred to as "orthogonal" fracture sets.

study is therefore to describe a method to calculate such effective properties based on some commonly observed fracture patterns.

Such natural fracture systems usually appear in one of two distinct types; so these networks can be defined by two parameters: intersection angle and fracture lengths. Intersection angles may be either right angles (Fig. 1) or dihedral angles (Fig. 2). Fracture patterns with right angles at these intersections are usually called "orthogonal" in geosciences with the assurance that both sets are opening mode fractures (Bai *et al.* [1]), whereas fracture sets having dihedral intersection angles require that the set formed first was later subjected to shearing (Pollard and Aydin [2]). Nevertheless, the sheared fracture set may also be represented as multi-collinear opening mode fractures for our present purposes.

When fracture systems in the earth become sufficiently dense, it is natural to study such systems using purely numerical methods. However, to gain some additional insight into the behavior of these systems, it should also be fruitful to have an analytical approach to study the elastic behavior as the fracture density increases, but before the system becomes mechanically unstable. One goal of the present work is to develop such analytical methods. To accomplish these goals, generalizations of the Backus [3] and Schoenberg and Muir [4] approaches are used to analyze layered systems, whose layers are intrinsically anisotropic due to any physical and/or mechanical mechanism. The pertinent mechanism considered here is due entirely to locally aligned fractures. By permitting the axis of symmetry of locally anisotropic compliance matrix/tensor for individual layers to differ from that of the layering direction, we derive

Figure 2. Field example of a fracture network composed of two or more sets of intersecting fractures having a dihedral (*i.e.*, oblique, or non-orthogonal) intersection angle between the fracture planes.

analytical formulas for interacting (*i.e.*, neighboring, but not intersecting) fractured regions with arbitrary orientations to each other. This procedure provides a convenient analytical tool for studying how contiguous, but not yet overlapping, fractured domains interact mechanically. The method also provides a straightforward means of predicting, via extrapolation, when and how such interactions might lead to more dramatic weakening effects, and ultimately to overall failure of these complicated systems.

Most of the detailed mathematical analysis of the paper is concentrated in the two Appendices (A and B). Section 2 introduces a definition of the fracture density that will be used throughout the paper. Section 3 provides further motivation for our chosen method of analysis. Section 4 gives a brief statement of the new method itself. Section 5 defines the crack-influence parameters which provide the analytical means of introducing fracture effects into the elastic layers. Section 6 presents some examples of the direct application of the methods developed. Section 7 gives a discussion of the main results. Section 8 makes use of these results to extrapolate to higher fracture densities at which levels the system might be expected either to fail, or to have already failed at some lower density due to mroe direct fracture-fracture interactions (such as interesections) not included in our present analysis. Section 9 gives a concise summary of the overall method, since it does include several fairly technically involved sub-steps of processing. Section 10 summarizes our overall conclusions. Some additional details of the mathematical routines used in this work are described in Appendices C and D.

2. FRACTURE DENSITY DEFINITIONS

It has been known since the paper of Bristow [5] that the pertinent fracture density that influences physical properties of fractured media such as resistivity and elasticity is *not* the fracture volume itself, but rather another related quantity that needs to be carefully defined. This fracture density does depend on the shape of the fracture. But, assuming thin fractures as we do here, it does not depend on this fracture thickness (or aspect ratio for ellipsoidal fractures) in a strong way.

Two terms commonly used to describe common geometries associated with cracks are: penny-shaped and ribbon-shaped. Penny-shaped cracks are cracks that have the approximate shape of an oblate (planetary) ellipsoidal hole in the material. Ribbon-shaped cracks are cracks that are more or less rectangular shaped holes, but possibly much longer in one dimension than the other of the rectangle – hence the name "ribbon-shaped." The third dimension in both cases is treated as small compared to the other two, but surely not identically zero, as then there would be no crack at all.

The easiest way to understand the pertinent fracture density is to start by studying what it is for ellipsoidal fractures, and for the physical property of resistivity. For an ellipsoid having equatorial radii a and b, and polar radius c, the volume of the ellipsoid differs from that of the fitted rectangular box (which is $V_r = 2a \times 2b \times 2c$), and is given by

$$V_e = \frac{4\pi}{3} \times abc. \tag{1}$$

When $a = b = c$, the standard result for volume of a sphere is: $4\pi a^3/3$. But this volume differs from that of a rectangular box in both cases (*i.e.*, both for the general ellipsoid and for a sphere) by a factor of $8/(4\pi/3) = 6/\pi \simeq 2$, with the rectangle/square solid figure being always about the same factor larger in volume than the ellipsoidal/sphere. Similarly, the area of the main face of an oblate spheroid is πab, whereas that for a rectangle is $4ab$, and that for a circle (with $a = b$) is πa^2. So the area of the fitted rectangular face is always larger by the factor $4/\pi$.

We will not go into more details here because they are spelled out perhaps with sufficient clarity in another recent paper [6], where Bristow's arguments were re-examined and updated somewhat by using modern theories, including Hashin-Shtrikman bounds [7, 8] that did not yet exist at the time of Bristow's work. Of course, the Hashin-Shtrikman bounds for multiphase materials [7] are not useful in the limit of thin cracks, since these bounds are typically based on inclusion volume, and this volume becomes very small for thin cracks. Therefore, volume of the crack itself is the wrong way to measure crack influence in many cracked systems, as has been shown by many authors including Bristow [6, 9, 10, 11, 12]. On the other hand, Hashin-Shtrikman bounds for polycrystals [8] do not suffer from the same limitations, since they are not based on volume fractions, but rather on random orientations of anisotropic crystals. Nevertheless, these bounds also have limitations since they implicitly require welded contacts between the crystalline grains composing the polycrystal. For applications to cracked systems, such assumptions are likely to be far from the reality of these fractured polycrystals, as the grain contacts are often precisely where some of the fractures are localized. In both types of Hashin-Shtrikman style results, the bounds can typically be too narrow, and in particular we would always expect a rigorous lower bound to be exactly zero — which, although also clearly a correct bound, is nevertheless not a useful result. In particular, the paper by Berryman and

Grechka [13] shows explicitly in the figures that the Hashin-Shtrikman bounds are much too narrow for the range of fractured systems being considered.

There has also been some recent controversy in the literature about the relative importance of crack-crack interaction versus non-interaction in different modeling methods for fractured systems [14, 15, 16]. These issues have not yet been resolved. So it is one purpose of the present paper to suggest a middle ground that seems quite appropriate for the types of geological systems of interest here. As we shall see, the present concept revolves around the idea that parallel cracks can be treated successfully as mostly noninteracting, while nonparallel cracks need to be treated differently. We establish this concept by introducing regions of parallel cracks contiguous to other regions of parallel cracks, but the two types of contiguous regions interact in ways to be established here due to the oblique angles between them — thus, leading to some significantly different interactions, as we shall show directly.

2.1. Penny-shaped cracks

The main idea of our analysis is quite simple, therefore, and is essentially this: The problems that concern us, whether resistivity or elasticity are basically at heart potential flow problems. Such problems can be understood using a fluid analogy, as has been known since the early work of Lord Kelvin [17] (also see, for example, Den Hartog [18] and Mehrabadi and Cowin [19]). For example, this ellipsoidal fracture is a nonconductive obstruction to the flow of current. In terms of potential theory, this picture is completely analogous to the hydrodynamic flow of fluid around an ellipsoidal solid obstruction. It is well-known that, if a thin disk oscillates in a fluid, it does so with an effective mass that is very different from the mass of the disk itself. This effective mass has to do with the fact that some of the surrounding fluid is entrained with the disk, and so the disk plus the entrained fluid becomes the effective object that is actually oscillating (to a good first approximation). We can look up results like this in Lamb's [20] textbook on *Hydrodynamics*. For a circular disk, the entrained fluid basically forms a sphere around the disk, and so the effective density of the disk is proportional ($\times 2/\pi$) to the corresponding density of the fitted sphere of volume $(4\pi/3) \times a^3$, when a is the radius of the circular disk. If the disk is not circular, but still ellipsoidal, then it turns out that the longest dimension is not so important because the fluid tends to flow around the disk by taking the path of least resistance — which involves significant potential flow mainly over the long sides, thereby creating a virtual cylinder of entrained fluid having the dimensions $2a \times 2a \times 2b$, if $b > a$, and volume $\simeq (4\pi/3)a^2b$ (approximately). This result is true even if the third dimension c (parallel to the main direction of flow) is very, very small compared to the other two dimensions, as it is for prolate spheroids or needles.

Analogous effects occur in both resistivity problems and elasticity problems, when fractures are introduced. These obstructions result in the same mathematical consequences for current flow and elastic potential flow in these geometrically related flow problems [17, 18, 20].

Thus, one convenient choice for effective fracture density in elasticity problems is given for a set of ellipsoidal fractures by:

$$\rho_e = (N/V)\frac{4\pi}{3}a^2b, \tag{2}$$

assuming that $c << a < b$. The ratio N/V is the number density (*i.e.*, number N per volume V). It is worth noting that, with the aspect ratio of the ellipsoids defined as $\alpha \equiv c/a$, the total

Table I. Induced mass factors $k_\perp$ and $k_\parallel$ for oblate (planetary) spheroids of aspect ratio α translating or oscillating in an ideal fluid (following Lamb [20], pp. 144–146, 700–701). The last column is presented as the product $k_\parallel \times \alpha$ because this is the physical quantity that remains finite as $\alpha \to 0$.

$\alpha = c/a$	$k_\perp$	$k_\parallel \alpha$
1	1/2	1/2
0.950	0.485	0.505
0.900	0.469	0.510
0.800	0.434	0.521
0.700	0.397	0.533
0.600	0.355	0.545
0.500	0.310	0.558
0.400	0.259	0.571
0.300	0.204	0.586
0.250	0.174	0.594
0.200	0.143	0.602
0.150	0.110	0.610
0.100	0.075	0.618
0.010	0.008	0.6347
0.001	0.001	0.6364
0	0	$2/\pi$

porosity due to fractures alone in this system is

$$\phi_e = (N/V)\frac{4\pi}{3}abc, \tag{3}$$

while the fracture density is given conveniently (and intuitively) by the ratio of the two dimensionless quantities, porosity and aspect ratio, as :

$$\rho_e = \phi_e/\alpha. \tag{4}$$

Some illustrative numerical values for oblate spheroidal fractures are presented in TABLE I.

2.2. Ribbon-shaped cracks

For rectangular or ribbon fractures, the ideas leading to an appropriate fracture density are very similar, but the final results take a different form. If a typical ribbon fracture has dimensions $h \times \ell \times t$, where h is height, ℓ is length, and t is effective thickness (of the resulting thin, flat hole), then the porosity of a set of such fractures is given – in a manner very similar to the earlier arguments – by

$$\phi_r = (N/V)h\ell t. \tag{5}$$

But the number density N/V is now measured in a different way: For ribbon fractures, we typically think in terms of spacing distance s between fractures. This distance might sometimes be taken to be an average spacing $\langle s \rangle$. Then, the spacing volume $v_r = V/N$ associated with each ribbon fracture (on average) is just $v_r \equiv h \times \ell \times \langle s \rangle$. So the porosity is simply

$$\phi_r = t/\langle s \rangle, \tag{6}$$

which is another intuitive result, since $t/\langle s \rangle$ is the fraction of the spacing distance occupied by the pores. The fracture density in this case is given now (since h is a diameter of the pertinent hydrodynamic cylinder, instead of being related to any fracture radius) by

$$\rho_r = (N/V)\frac{\pi h^2}{4} \times \ell = \pi h/4 \langle s \rangle = \pi \phi_r/(4t/h). \tag{7}$$

Noting that this factor $\pi/4$ is of order unity, we can choose to ignore it, or not, as a matter of personal preference when defining the fracture density. Except for such factors of order unity, this result agrees (for example) with the lecture notes of Thomsen [21], and both qualitatively and semi-quantitatively with very similar discussions of fracture density by Budiansky and O'Connell [9].

3. MOTIVATION FOR THIS APPROACH

Now our primary purpose is to produce semi-analytical estimates of quasi-static elastic moduli for slowly evolving fractured systems. The basic idea is therefore to find means of obtaining quantitative measures that are valid up a point just prior to that at which significant qualitative changes take place — an example of which is the coalesence of smaller fractures into larger fractures (which may in turn result in significant nonlinear behavior, up to and including system failure, by which we mean here that one or more of the system stiffness eigenvalues vanishes). Achieving this goal will require somewhat delicate analysis, and so we are careful *not* to attempt to push it beyond the realm where it is obviously still valid. To implement the quasi-static averaging method, we make use of the early work of Backus [3], as well as more recent work of Schoenberg and Muir [4]. (Also see Milton [22].) Both of the primary works have similar goals: in particular, the use of their two formalisms to describe elastic moduli pertinent to long wavelength seismic waves. Our present goal differs somewhat from theirs, since we intend to apply very similar means to the study of quasi-statics and slow fracture evolution in a structural geology setting.

Whether studying stiffness or compliance, we typically use a well-known (Voigt [23], Nye [24], Mehrabadi and Cowin [19]) prescription for transforming back and forth between tensor and matrix notation. (At a later point in the analysis, we must also introduce the Kelvin form [17, 19] of the elastic matrix — see Appendix C for a definition — for reasons that will become apparent.) For studies of wave propagation, it is usually preferable to study stiffnesses, which in the seismological community are typically represented by coefficients C_{ij} of the six-by-six stiffness matrix $\mathbf{C}$ (which is just the Voigt simplification of the corresponding fourth-rank tensor). We will also use this Voigt six-by-six matrix approach, but instead of concentrating on the stiffness, we consider its inverse S_{ij}, which is the six-by-six compliance matrix $\mathbf{S}$.

There are two important reasons for using the compliance version of the method, instead of the stiffness version: (1) The system we choose to study has uniform background material, perhaps isotropic (although this is not an essential feature of the method), to which oriented fractures are added. Once added, these oriented fractures cause the system to become locally anisotropic, which is exactly what we want to study. Adding fractures is most easily and naturally done throughout our analysis by adding the effects of such holes/fractures via the compliance moduli S_{ij}. Holes introduce increased compliance through a linear mechanism (Kachanov [25], Sayers and Kachanov [26]) in the compliance matrix (or tensor), but the same

holes would instead provide a nonlinear decrease in the stiffness matrix (or tensor). (2) The second reason for studying the analysis from the compliance point of view is that we can save some steps later in our analysis, because the quantities that appear naturally this way are Young's moduli (E), Poisson's ratios (ν), and shear moduli (G). Young's moduli and shear moduli will appear as inverse moduli along the matrix diagonal of the final results, while the Poisson's ratios are also most easily obtained from the off-diagonal components once the Young's moduli along the diagonal have been determined. Thus, we may sometimes avoid one comparatively tedious step of matrix (tensor) inversion by the present choice of formulation. There is nothing else fundamentally different in our chosen technical approach from that of Backus [3] and/or Schoenberg and Muir [4], but our goals — and therefore our desired results — take us in somewhat different directions.

4. QUASI-STATIC MODULI FOR COMPLICATED CRACKED SYSTEMS

We study systems that have fairly high densities of oriented (by which we mean here "aligned" or "parallel") fractures, and that have two (or more if desired) such systems that are differently oriented, but nevertheless contiguous, but also nonintersecting. One semi-analytical way of dealing with such systems is to treat them as if they are locally layered (see Fig. 3). Each layer may be considered homogeneous (though still anisotropic), because it contains only fractures having just one and the same orientation. So each layer can be "homogenized" to produce effective elastic constants for that layer. These constants will be determined to some extent by the axis of symmetry, but this axis will not necessarily (and for the present analysis *usually* will not) be aligned with the direction of the layering itself. Figure 3 shows one example of the type of layered systems we have in mind. The angle between the oriented fractures in the two layers shown can be considered arbitrary, but we purposely design the layered system itself for this analysis so that we can take advantage of the symmetry gained by aligning the fractures. Then, the angular difference between the two layers is split exactly evenly between the two layers. This approach takes maximal advantage of the symmetry, and also of the fact that the layer-averaging method treats the boundaries between layers in a special way: namely, that these boundaries are "welded." This term means that, after the rotations, fractures in this model do not ever appear parallel to these boundaries, and especially (most importantly) not aligned right along the boundaries between the layers.

The layer-averaging scheme assumes that strains at these boundaries and in the planes of the boundaries (*i.e.*, ϵ_{11}, ϵ_{22}, and ϵ_{12}) are continuous, and also that the corresponding stresses are also continuous for components such as normal stress (say σ_{33}) and torsional shear stresses (say σ_{13} and σ_{23}) perpendicular to the in-plane directions 2 and 1, respectively. Continuity of the remaining components of stress and strain is not guaranteed, but also not prohibited. But these particular jumps across the boundaries are physically nd mechanically correct in all cases.

The formulation of the mathematical problem for elastic layers themselves is somewhat different from previous treatments (for compliance rather than stiffness), but basically obtained using a rather minor modification of earlier work by Backus [3] and also by Schoenberg and Muir [4]. So this method is summarized here as review material in Appendices A and B.

One clearly artificial aspect of this approach is the assumption that the crack densities in the layers are all identical in magnitude. We make this restrictive choice to simplify the modeling
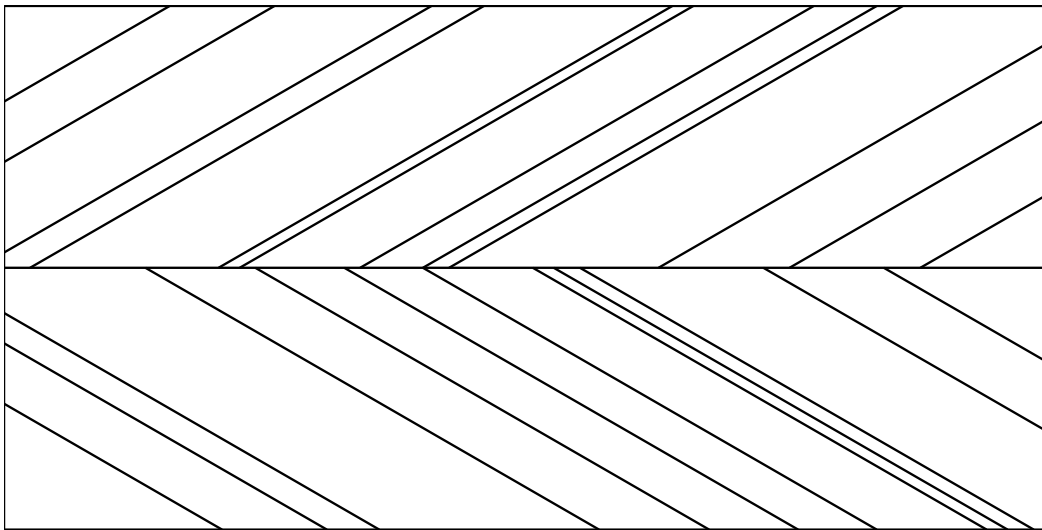
Figure 3. Example of a side view of the main type of layered medium considered in the text. The layers are stacked top to bottom with only two of these types of layers being shown. Individual layers being fractured/fractured, each have the same fracture density but not necessarily exactly the same fracture distribution. For the example shown, the planes of the flat fractures are all at either $\pm30^{o}$ from the planes of intersection. All fractures in a given layer have the same angular orientation. Cracks are seen here edge on.

in a first treatment. Certainly this constraint can be relaxed, as there is no such requirement imposed by the layer-averaging method itself, which is general and therefore can handle any combination of different types of layers.

5. DEFINITION OF THE CRACK-INFLUENCE PARAMETERS

The main idea we use in order to quantify the effects of cracks distributed either randomly or in an organized way in an otherwise elastic material is based on work of Kachanov [25]. This work introduced an elastic potential energy that is quadratic in the stress tensor and that can be expressed in terms of invariants of the stress tensor in various combinations involving the "crack density tensor." This method results in a fairly complicated energy potential function involving nine distinct terms, seven of which characterize the influence of a dense crack distribution on an isotropic (background or host) elastic medium. But this function has the advantage that, upon linearization in the crack density, it reduces to only four terms. Two of these terms are the standard ones for the pure (uncracked) medium and the remaining two terms contain the linear contributions (increases in compliance) due to the cracks. Sayers and Kachanov [26] introduced a very useful scheme based on these ideas that enables the calculation of constants for anisotropic cracked media from estimates of the behavior for the isotropic case. This approach is a great simplification of a difficult technical problem. Now it is also not obvious that linearization is permissible in all the crack density ranges of interest, but Sayers

and Kachanov [27] showed in later work that the remaining contributions from the fourth rank crack-density tensor are often small — and therefore negligible in many situations of practical interest. The neglect of these terms nevertheless implies a certain amount of error in any calculation made based on their absence. But — if this error is of the size of our measurement error or less — it should not be a serious impediment to studies and analysis of these systems.

We make use of standard Voigt definition of the compliance matrix $\mathbf{S}$ as displayed in Appendix A, Eq. (18).

A simple example shows that the first order corrections to the compliance tensor — using the Voigt 6×6 matrix notation S_{ij} — due to the presence of a low crack density ρ_c and an isotropic distribution of similarly shaped small cracks take the form:

$$\Delta S_{ij}^{(1)} = \rho_c \begin{pmatrix} 2(\eta_1+\eta_2)/3 & 2\eta_1/3 & 2\eta_1/3 & & & \\ 2\eta_1/3 & 2(\eta_1+\eta_2)/3 & 2\eta_1/3 & & & \\ 2\eta_1/3 & 2\eta_1/3 & 2(\eta_1+\eta_2)/3 & & & \\ & & & 4\eta_2/3 & & \\ & & & & 4\eta_2/3 & \\ & & & & & 4\eta_2/3 \end{pmatrix}, \quad (8)$$

where η_1 and η_2 are the first two coefficients appearing at lowest order in ρ_c for the Sayers and Kachanov [26] theory. For example, $\rho_c = Nb^3/V$ is the crack density (here N/V is the number density and b is the radius of the flat cracks when they are penny-shaped). These two coefficients can be determined for any crack density by computing the analytical form of the bulk and shear moduli from the compliance matrix $S_{ij}^* = S_{ij} + \Delta S_{ij}$, and then comparing the results one-to-one with the results from any effective medium theory one trusts. For these purposes, the differential scheme (DS) is the one that Sayers and Kachanov [26] chose to use, but other choices can also be made. It is known that the value of the magnitude $|\eta_1|$ is generally much smaller than that of η_2. In particular, $|\eta_1/\eta_2| \leq 0.01$ is typical of the results obtained from the most commonly used effective medium theories.

The advantage of this approach can now be demonstrated very simply by considering a pertinent example. If all the cracks in the system have the same vertical (z-)axis of symmetry, then the cracked/fractured system is not isotropic, and we have the first-order compliance correction matrix for horizontal fractures is:

$$\Delta S_{ij}^{(1)} = \rho_c \begin{pmatrix} 0 & 0 & \eta_1 & & & \\ 0 & 0 & \eta_1 & & & \\ \eta_1 & \eta_1 & 2(\eta_1+\eta_2) & & & \\ & & & 2\eta_2 & & \\ & & & & 2\eta_2 & \\ & & & & & 0 \end{pmatrix}. \quad (9)$$

It is not difficult to see that, if the cracks were oriented instead so that all their normals were pointed horizontally along the x-axis, then we have one permutation of this matrix and, if instead they were all pointed horizontally along the y-axis, then we have a third permutation of the matrix. If we then want to understand the isotropic correction matrix in (8), we can just average these three permutations: *i.e.*, simply add the three ΔS's together and then divide by three. Having done that, we exactly recover the isotropic compliance corrections matrix displayed in (8). This construction shows in part both the power and the simplicity of the Sayers and Kachanov [26] approach, and how the neglect of small nonlinear terms leads naturally to useful linearization techniques.

6. SOME EXAMPLES USING THE METHOD

For our present application, we need estimates first of the effects of fractures on the compliances **S** of the elastic systems of interest. Using the methods of Sayers and Kachanov [26], the paper of Berryman and Grechka [13] shows how to obtain such estimates of fracture effects, together with a specially designed fitting method for the numerical simulation results of Grechka and Kachanov [14]. These results provide the values that we need to use in the explicit model analysis that follows.

6.1. An explicit example

For final results, we also need a broad range of values from our fracture density simulations. Such results are readily available for fracture densities up to $\rho = 0.2$ in the paper by Berryman and Grechka [13]. We illustrate the approach with just one explicit example (but many more were treated while developing the Figures that follow). Results of Berryman and Grechka [13] lead to the conclusion that the effective compliance matrix for oriented fractures at the fracture density $\rho = 0.10$, when the fractures are imbedded in a sandstone-like medium such as the one studied in that paper having Poisson's ratio $\nu \simeq 0.4375$, should be given approximately in units of GPa^{-1} by

$$\mathbf{S} = \begin{pmatrix} 0.15810 & -0.06917 & -0.07109 & & & \\ -0.06917 & 0.15810 & -0.07109 & & & \\ -0.07109 & -0.07109 & 0.21764 & & & \\ & & & 0.50549 & & \\ & & & & 0.50549 & \\ & & & & & 0.45455 \end{pmatrix}, \qquad (10)$$

based on extensive numerical simulations (hundreds of examples of interacting cracks were studied) by Grechka and Kachanov [14]. This case corresponds to an elastic system having Young's moduli $E_{11} = E_{22} = 6.3251$, $E_{33} = 4.5947$ GPa, and torsional shear moduli $G_{44} = G_{55} = 1.9783$, $G_{66} = 2.2000$ GPa. Blanks in the matrix are zeroes.

The fracture influence parameters (in units of GPa^{-1}) used to arrive at (10) are: $\eta_1(0) = -0.0192$, $\eta_2(0) = 0.3994$, $\eta_3(0) = -1.3750$, $\eta_4(0) = 0.0000$, and $\eta_5(0) = 0.5500$. Coefficients η_1 and η_2 contribute to the compliance results after multiplication by ρ to the first power. Coefficients η_3 and η_5 contribute to the compliance results after multiplication by ρ to the second power. Coefficient η_4 was found not to influence the results in any significant way, so its value is neglected. Higher powers of ρ than the second power were not treated in Berryman and Grechka [13], as the numerical data used in the fitting procedure stopped at $\rho = 0.20$, and fitting higher order coefficients to a satisfactory level of accuracy requires numerical data at ρ values higher than 0.20, which were unfortunately not available at that time.

Now we want to study the effects when at least two sets of fractures are present; these fractures are locally oriented, but contiguous groupings of fractures (in different layers in our model) have different orientations, with angles of near-intersection at either dihedral or right angles as shown previously in the photographs of natural fractures in Figs. 1 and 2. We treat this aspect of the problem by rotating the fracture orientation in five distinct cases, so that two sets of fractures have orientations that differ by $\Theta_F = 15^o$, 30°, 45°, 60°, and 90°. We accomplish this by rotating one set by half the total angle in one direction, and the other set by half the total angle in the opposite direction: $\pm 7.5^o$, $\pm 15^o$, 22.5^o, $\pm 30^o$, $\pm 45^o$. (See Fig. 3.)

Table II. Values of three eigenvalues of stiffness and their sum for the layered system as a function of fracture density ρ and rotation angle Θ_F.

ρ	Θ_F	$3qK$ (GPa)	$2qG_p$ (GPa)	$2qG_u$ (GPa)	Sum (GPa)
0.00	all	50.60	4.40	4.40	59.40
0.05	0°	34.86	4.40	3.97	43.22
	15°	34.79	4.40	3.97	43.16
	30°	34.61	4.38	4.01	43.00
	45°	34.38	4.37	4.05	42.80
	60°	34.15	4.33	4.11	42.59
	90°	33.92	4.28	4.19	42.39
0.10	0°	29.49	4.40	3.67	37.55
	15°	29.36	4.39	3.68	37.44
	30°	29.02	4.37	3.72	37.11
	45°	28.57	4.32	3.78	36.67
	60°	28.12	4.27	3.85	36.24
	90°	27.69	3.96	4.19	35.84
0.20	0°	26.75	4.40	3.38	34.53
	15°	26.55	4.38	3.39	34.31
	30°	26.00	4.32	3.40	33.72
	45°	25.32	4.25	3.41	32.98
	60°	24.69	4.17	3.43	32.29
	90°	24.11	3.45	4.08	31.65

To perform the actual matrix rotation, we use methods and codes supplied online by Dellinger [28]. These codes assume input of stiffness matrices and then provide output also in the form of stiffness matrices. So we first invert the compliance matrices shown into stiffness matrices, and then — after the rotation — we invert them back into our desired compliance form. [*Technical Note:* We need to perform these extra steps because the eigenvalue structure of the stiffness matrices is preserved correctly in Dellinger's codes for the stiffnesses, but — because of differences in Voigt matrix structures for stiffness and compliance matrices (see Nye [24]) — the eigenvalue structure for compliances is unfortunately not preserved.]

For example, after the unrotated stiffness matrix is known from the inversion step, we can use the rotation code, and find that the rotated stiffness matrix for a rotation angle (for example) of $+15^o$ around the x-axis (or 1-axis, or x_1-axis) is:

$$\mathbf{C'} = \begin{pmatrix} 13.97 & 9.442 & 7.814 & -0.47 & & \\ 9.442 & 13.66 & 7.706 & -0.576 & & \\ 7.814 & 7.706 & 9.89 & -0.512 & & \\ -0.47 & -0.576 & -0.512 & 1.997 & & \\ & & & & 1.993 & -0.055 \\ & & & & -0.055 & 2.185 \end{pmatrix}. \tag{11}$$

For comparison purposes, consider that the sum $c_{11} + c_{22} + c_{33} = 37.52$ GPa and note that for the unrotated case, the corresponding trace value ($\equiv$ Sum) in TABLE II is 37.55 GPa. Since the layer-average result for the pertinent rotation value of 30° is $c_{11} + c_{22} + c_{33} = 37.11$ GPa, we see that there is a decline in overall stiffness due to these combined rotations and

layer-averages, but this decline is really quite small.

Then, after using results of Appendix C again to invert this matrix back to compliance form, the resulting rotated compliance matrix is:

$$
\mathbf{S}' = \left(
\begin{array}{cccccc}
0.15805 & -0.06926 & -0.07096 & & & \\
-0.06926 & 0.25340 & -0.07029 & & & \\
-0.07096 & -0.07029 & 0.21285 & & & \\
& & & 0.50855 & & \\
& & & & 0.50211 & 0.01274 \\
& & & & 0.01274 & 0.45799
\end{array}
\right). \tag{12}
$$

This result corresponds to an elastic system having Young's moduli $E_{11} = 6.3272$, $E_{22} = 6.2019$, $E_{33} = 4.6981$ GPa, and torsional shear moduli $G_{44} = 1.9664$, $G_{55} = 1.9916$, $G_{66} = 2.1835$ GPa. When the rotation is performed in the opposite direction (*i.e.*, -15°), the only difference in the resulting compliance matrix is that the off-diagonal terms $S_{56} = S_{65}$ have opposite signs. All the other coefficients remain exactly the same. This exact type of symmetric behavior was observed to be characteristic of all the examples considered here, and shows explicitly why orthorhombic systems are important and ubiquitous in fractured media.

Figure 4 shows results for effective Young's moduli E_{11}, E_{22}, E_{33}, and shear moduli G_{44}, G_{55}, G_{66}, for $\rho = 0.05, 0.10$ and 0.20. Angles considered form a subset in the range $\Theta_F = 0^o$ to 90°. One general characteristic we observe is that, for $\Theta_F = 0^o$, $E_{11} = E_{22}$ and $G_{44} = G_{55}$ – behavior corresponding to transversely isotropic (TI) media with symmetry axis $x_3 = z$. Similarly, for $\Theta_F = 90^o$, $E_{22} = E_{33}$ and $G_{55} = G_{66}$ – corresponding to transversely isotropic (TI) media having symmetry axis $x_1 = x$. This transition is entirely expected, since the rotations are all performed around the x-axis.

Figure 5 shows that the weakening of the system for the Young's moduli E_{11}, E_{22}, E_{33} and also for the torsional shear modes G_{44}, G_{55}, G_{66} ranges from an 11% to 20% effect for G_{44} and G_{55}, while the effect on G_{66} ranges from being negligible up to about 11%.

The effect of rotations on Young's modulus E_{11} is zero at all angles and all fracture densities, since the rotations are all performed around the x-axis. Changes in the modulus E_{22} carry it from the values of E_{11} to those of E_{33}, as the rotation angle changes from 0° to 90°. E_{33} is the most interesting case, having lost from 24% to 33% of its initial value, depending on the magnitude of the rotation angle.

Figure 6 displays the results for the three "quasi-modes" (this term is defined carefully in the following three paragraphs) of elastic response: qK, qG_p, and qG_u. These modes are true eigenvalues [11] of the layer-averaged system, but they are nevertheless not so easily identified in terms of bulk and shear modulus, or compressional and torsional behavior. Relating the symbols to actual eigenvalues $\lambda_1, \lambda_2, \lambda_3$, we can express these three quasi-moduli as $qK = 1/3\lambda_1$ for the quasi-bulk modulus, $qG_p = 1/2\lambda_2$ for the quasi-pure shear modulus, and $qG_u = 1/2\lambda_3$ for the quasi-uniaxial shear modulus. The values $\lambda_1, \lambda_2, \lambda_3$ are the three eigenvalues of the 3×3 matrix in the upper left corner of the compliance matrix S_{ij} for the layered system. As a rule, we found it was not at all difficult to determine which of these modes was which in the cases considered in our examples. The only problematic region is that around $\Theta_F \simeq 75^o$, where the values of qG_p and qG_u become comparable and then crossover. These two eigenvalue branches actually change character form pure to uniaxial shear in this region. This region is therefore more difficult to treat carefully than the rest of those treated in the paper, so we are not showing these details in the present work.

Figure 4. Effective Young's moduli and torsional shear moduli, respectively, overall for the layered systems considered: (a) and (b) are for $\rho = 0.05$, (c) and (d) are for $\rho = 0.10$, (e) and (f) are for $\rho = 0.20$ fracture densities. Note that these results indicate transversely isotropic symmetry, but having different (and orthogonal) axes of symmetry at $\Theta_F = 0^o$ and 90°.

6.2. Motivating the quasi-modes

For comparison, it is common in the seismic wave and acoustic wave propagation literatures to call the three wave modes that are actually dependent on these same moduli, respectively, the quasi-compressional or quasi-P wave, the quasi-SV wave (meaning shear wave with vertical plane of polarization), and the SH wave (for the shear wave having horizontal plane of
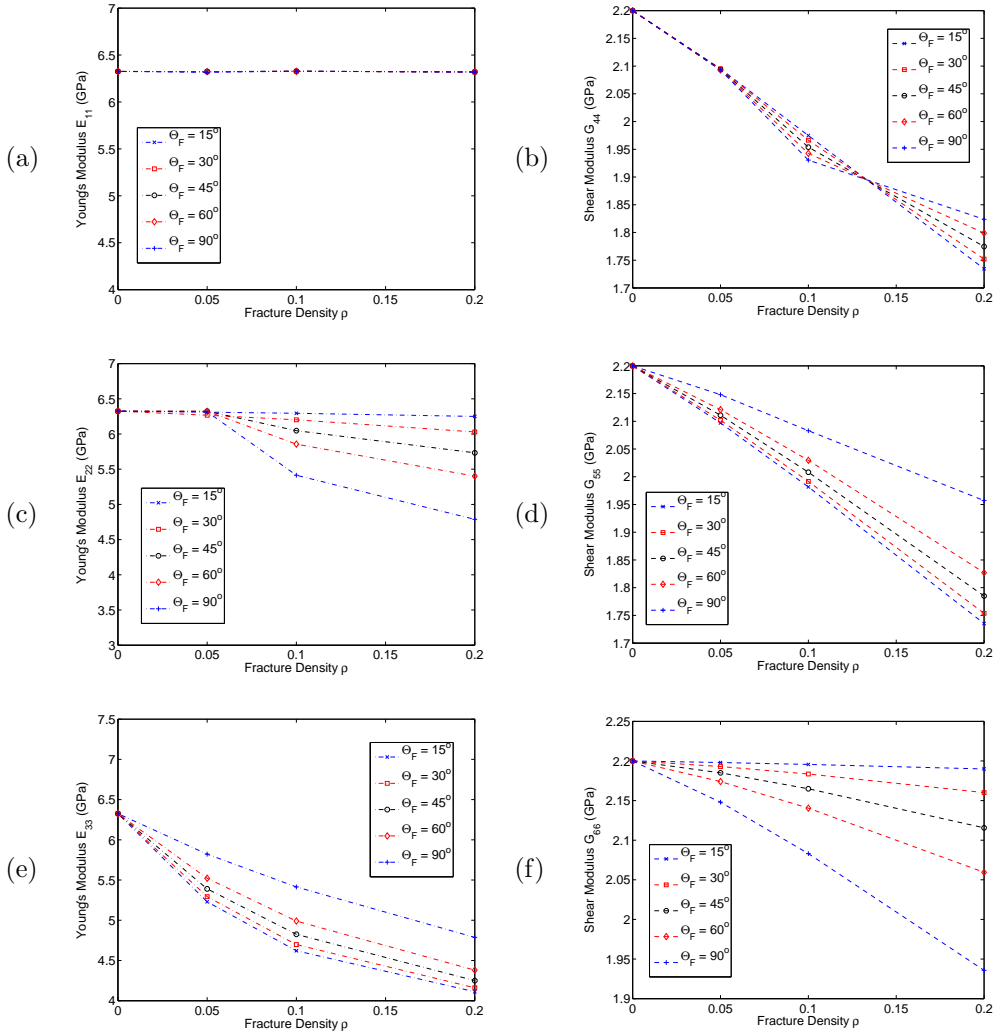
Figure 5. Effective Young's moduli E and torsional shear moduli G, respectively, for the layered systems considered to a fracture density of $\rho = 0.2$: (a) E_{11}, (b) G_{44}, (c) E_{22}, (d) G_{55}, (e) E_{33}, and (f) G_{66}. Relative orientations of the fractures in different layers for the five cases are: $\Theta_F = 15^o$, 30°, 45°, 60°, and 90°. For the orthorhombic systems considered, these torsional shear moduli are three of the six eigenvalues for the elastic response. The other three eigenvalues are presented separately in Figs. 8 and 9.

polarization). For present purposes, these designations are not directly pertinent. But we can nevertheless define three quasi-modes having these effective moduli: the quasi-bulk modulus qK, the quasi-pure shear modulus qG_p, and the quasi-uniaxial shear modulus qG_u. The quasi-compressional mode having eigenvalue qK is found to be the only one of the three modes having all three components in the corresponding eigenvector of the same sign. A true bulk
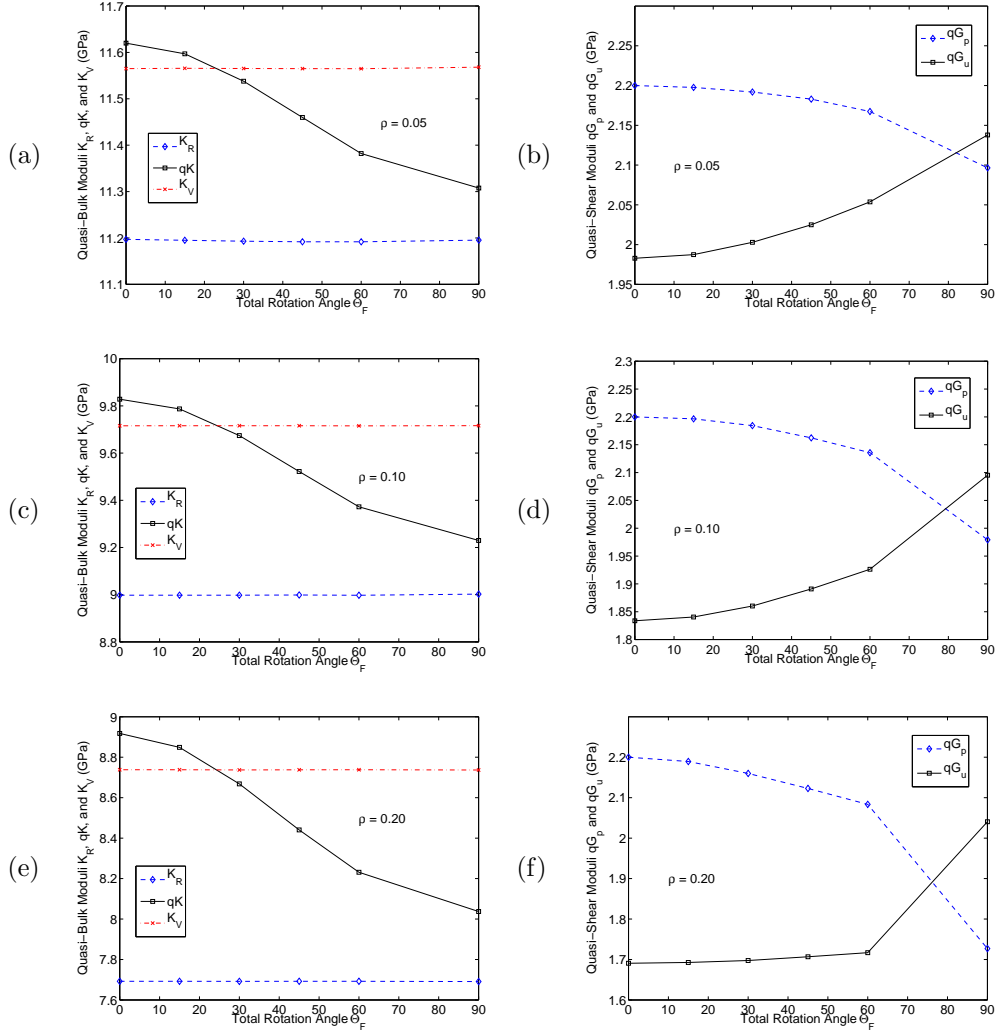
Figure 6. Quasi-bulk moduli, qK and K_R, and quasi-shear moduli, qG_p and qG_u, for the layered systems considered: (a) and (b) are for $\rho = 0.05$, (c) and (d) are for $\rho = 0.10$, (e) and (f) are for $\rho = 0.2$ fracture densities. Note the change of character in the qG_p and qG_u, which results in the crossing of these curves in (b), (d), and (f) for large Θ_F.

modulus mode would have all three components of the eigenvector equal in magnitude and also of the same sign. However, this hydrostatic state is usually not an eigenmode for most anisotropic elastic media. (Cubic symmetry media provide one anisotropic counter-example to this otherwise general statement.)

The quasi-pure shear modulus qG_p corresponds to a mode with one eigenvector component significantly smaller than the other two, and these two are comparable in magnitude, but

opposite in sign. A true pure-shear mode would have one component exactly zero, and the other two of equal magnitude, but opposite sign. TABLE III presents some examples of the observed results for this mode. In particular, it is seen here that this mode is exactly of the pure-shear type, having eigenvectors $(1, -1, 0)/\sqrt{2}$ and $(0, -1, 1)/\sqrt{2}$, respectively, for $\Theta_F = 0^o$ and $\Theta_F = 90^o$.

The remaining mode has eigenvalue qG_u, and is termed the quasi-uniaxial shear mode. A true uniaxial shear mode [29, 30] is the eigenmode remaining when an applied uniaxial compression (or tension) is decomposed into a pure hydrostatic compression (or tension), and a shear mode. Thus, in pure uniaxial-shear, the stresses satisfy $\sigma_{33} = -2\sigma_{11} = -2\sigma_{22}$, or the equivalent statement for strain, and/or any appropriate permutations of the indices 1,2,3. The quasi-uniaxial mode is therefore the only one having two components of comparable magnitude and also the same sign, while the third component is of opposite sign, and approximately twice the magnitude of the other two.

In general we have also found that both the Reuss average K_R and the Voigt average K_V bulk moduli were nearly constant, as a function of the rotation angle Θ_F [30] for fixed fracture density ρ. Hill [31] has shown that these effective moduli are lower and upper bounds respectively on the true effective bulk modulus that can be defined for such anisotropic systems. Hill's average is either the arithmetic or geometric mean of K_R and K_V, although experience shows that the arithmetic mean usually fits rock data better.

The quasi-uniaxial shear modulus qG_u is the smaller of the two quasi-shear modes, but it also tends to increase with rotation angle. The quasi-bulk modulus qK and the quasi-pure shear modulus qG_p were both variable, and showed qualitatively very similar behavior over the range of values considered. However, the quantitative behavior of these two modes was quite different, as the quasi-bulk modulus declined from 5 to 10% in value, whereas the quasi-pure shear modulus lost from 5 to 25% of its initial value as the rotation range varied from 0° to 90°, depending on the fracture density value. The quasi-pure shear mode is therefore the one that is most strongly influenced by the angle between the fracture sets in the two types of layers considered in our modeling.

The torsional shear moduli G_{44} and G_{55} both behave similarly to qG_u, while G_{66} behaves similarly to qG_p. Overall decrease in modulus magnitude as ρ increases (see Fig. 9) is about the same in all the shear modes, although G_{66} and some of the smaller rotation angles for qG_p result in slower fall off in these shear modulus values.

7. DISCUSSION

Figure 3 shows the concept being used in the sets of examples in Figs. 4–7. The results from Appendices A and B were used to generate numerical estimates of six effective layer-averaged compliances (specifically, the diagonal components of **S**): $1/E_{11}$, $1/E_{22}$, $1/E_{33}$, $1/G_{44}$, $1/G_{55}$, and $1/G_{66}$. Results in (a) and (b) were generated for rotations of the fractures to angles $\pm 15^o$, so the total angle Θ_F between the fractures in the layers is 30°. Similarly, for (c) and (d), the angles were $\pm 30^o$ of rotation and $\Theta_F = 60^o$ relative to each other; and, for (e) and (f), the angles were $\pm 45^o$ of rotation and, therefore, relative fracture angle $\Theta_F = 90^o$.

[*Technical Note:* We have only used available numerical data at the four fracture densities: $\rho = 0.0, 0.05, 0.10$, and 0.20. That is why the curves shown typically have breaks in curvature at these particular values of fracture density in Figs. 5 and 7.]

Table III. Compliance eigenvalues $x_2 \equiv \frac{1}{2(qG_p)}$ and normalized eigenvectors (α, β, γ) for the quasi-pure shear mode at various values of the fracture density ρ and rotation angle Θ_F.

ρ	Θ_F	x_2 (GPa^{-1})	(α, β, γ)
0.05	0°	0.22727	$(0.70711, -0.70711, 0.00000)$
	15°	0.22751	$(0.70551, -0.70870, 0.00147)$
	45°	0.22905	$(0.69996, -0.71418, -0.00240)$
	60°	0.23069	$(0.70712, -0.70638, -0.03181)$
	90°	0.23849	$(0.00000, -0.70711, 0.70711)$
0.10	0°	0.22727	$(0.70711, -0.70711, 0.00000)$
	15°	0.22763	$(0.70656, -0.70764, -0.00307)$
	45°	0.22245	$(0.66009, -0.74663, 0.08262)$
	60°	0.23411	$(0.71692, -0.69136, -0.08969)$
	90°	0.25263	$(-0.00082, -0.70655, 0.70766)$
0.20	0°	0.22727	$(0.70711, -0.70711, 0.00000)$
	15°	0.22838	$(0.70801, -0.70612, -0.01045)$
	45°	0.23553	$(0.72207, -0.68251, -0.11310)$
	60°	0.23999	$(0.73577, -0.64484, -0.20697)$
	90°	0.28952	$(0.00000, -0.70711, 0.70711)$
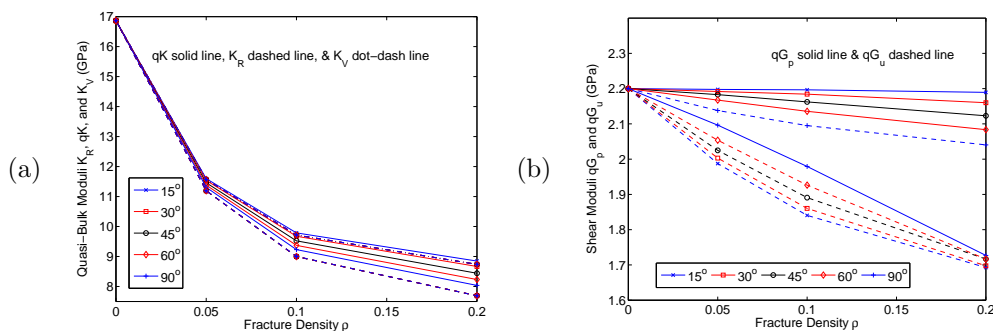
Figure 7. Quasi-bulk moduli, qK, K_R, and K_V, are displayed in (a) and the quasi-shear moduli, qG_p and qG_u are displayed in (b), for the rotation angles considered in the text. The Reuss average K_R is a rigorous lower bound on effective bulk modulus, while the Voigt average K_V is a rigorous upper bound. Although the quasi-bulk modulus qK is a rigorous eigenvalue of the elastic system under study, it is not necessarily simply related to an overall effective bulk modulus of the composite system.

The changes in Young's moduli (E) are relatively straightforward to explain: For each Young's modulus, the main issue is how much the presence of one fracture, or one set of similarly oriented fractures, changes the compliance in the given direction. The situation for E_{11} is very simple, as it does not ever change as the angle between these fractures change. This modulus depends on ρ, but otherwise is clearly independent of the presence of the fracture-angle changes as it should be, since the fracture rotations are all being performed around the

x-axis.

So $1/E_{11}$ is the compliance directly into the diagram in Fig. 3, *i.e.*, normal to the printed page. The presence of the fractures has minimal (actually negligible) effect in this direction on Young's modulus E. On the other hand, it has its greatest effect on E_{33}, since this is the modulus pertinent to the layering direction in Fig. 3. The effect is already quite large at $\Theta_F = 30^o$, and only increases slightly as the angle continues increasing up to $\Theta_F = 90^o$. In contrast, the effect of the increasing angle on E_{22} is intermediate between the effects on E_{11} and E_{33}, until the angle reaches $\Theta_F = 90^o$, at which point is is clear that $E_{22} \equiv E_{33}$ is a requirement (as observed), since the two oppositely rotated fracture sets are now exactly orthogonal to each other at this point (producing a distinctly different TI medium from the one for $\Theta_F = 0^o$, in which case all the fractures are still parallel to each other). So stresses in the z-direction or in the y-direction both experience exactly the same environment, and therefore we must also see the same elastic response.

8. SUMMARY OF MAIN METHOD

Since the methods of analysis presented so far have multiple steps, each of which has its own inherent complications and associated questions, it seems appropriate to reprise these steps and attempt to summarize what has been accomplished at this point.

First, we applied the Sayers and Kachanov [26] method, using fracture influence coefficients obtained peviously in the work of Berryman and Grechka [13], and based upon results from numerical simulations by Grechka and Kachanov [14]. This step is the only one that introduces fractures into our effective medium model system. So this is the only step that explicitly makes use of fractures to weaken the elastic matrix, while simultaneously introducing anisotropy — due to the fact that the fractures introduced are all locally aligned within a layer — into the otherwise isotropic elastic background medium.

Second, we rotate the axes of the system of aligned fractures twice: each time the rotation is about the x-axis (for a system originally having z-axis of symmetry). One of these rotations is positive $(+\theta)$, and the other negative $(-\theta)$ — both being of exactly the same magnitude. These two rotations do nothing in themselves to weaken or strengthen the previously fractured systems that become the layers of the model. Because rotations of the axes do not change either the trace or the determinant of a matrix, taking these actions leaves the eigenvalues of each rotated matrix completely unchanged. It is observed however that the positive and negative rotations do change the values in the matrices in the upper left 3×3 corner of the matrix, and also along the diagonal of the lower right 3×3 submatrix. Furthermore, these rotations produce nearly identical matrices overall, the only differences being in certain off-diagonal components, nonzero values not previously present in the unrotated matrices. Furthermore, these new matrix elements all have opposite signs, by which we mean that the ones that have $\pm$ signs for the positive rotation have $\mp$ signs for the negative rotation. (This particular result is special for equal angular rotations combined with equal crack densities. The current method can certainly be generalized in this regard, but the results then become cumbersome to tabulate – *i.e.*, multidimensional results for different angles and/or different crack densities. So this extension was beyond our current scope.)

The third step then involves stacking these two rotated systems and using the Backus [3] or Schoenberg-Muir [4] layer-averaging methods to determine the effective properties of the

resulting composite system. One remarkable fact discovered is that those new off-diagonal terms (and this would also be true even for off-off-diagonal terms if they occurred at a non-negligible magnitude) introduced in the second step exactly cancel out in the layer-averaging process, *i.e.*, they layer-average exactly to zero. Therefore, we are always left with an orthorhombic system having fractures located relative to each other at twice the magnitude of the original rotation angles [$2 \times \theta = \Theta_F$].

This final orthorhombic anisotropic elastic system compliance matrix is relatively easy to analyze, and the results show that there is one mode (out of six) of this system that is always the weakest one. This mode is the one we have termed the quasi-pure shear mode, having effective eigenvalue qG_p. This mode has the characteristic that, of the three eigenmodes in the upper left 3×3 of the matrix, it is the one closest to that of a pure shear (*i.e.*, $\sigma_{11} = -\sigma_{22}$, while $\sigma_{33} = 0$). The other two quasi-modes are a quasi-bulk mode closest to $\sigma_{11} = \sigma_{22} = \sigma_{33}$, and a quasi-uniaxial shear mode closest to $\sigma_{33} = -2\sigma_{11} = -2\sigma_{22}$. Both of the other two quasi-modes have modest changes in modulus values as rotation angle changes from 0° to 90°.

Because the resulting effective medium system (for the special choices made here) is generally orthorhombic, there are three more shear modes, and these correspond to the three torsional shear modes of the system. These modes are the ones associated specifically with the torsional shear moduli G_{44}, G_{55}, and G_{66}. Of these three moduli, the shear modulus G_{44} changes least with rotation angle. The two shear moduli G_{55} and G_{66} do change more substantially, however, with G_{55} generally increasing in value while G_{66} decreases. The observed increase seen in G_{55} is essentially required for this system of equations, because of the fact that both the trace and determinant of the rotated matrices in the second step must have (because of the invariance of these quantities for all matrices) constant values before and after the rotations.

So, if any of the eigenvalues goes down due to the rotations (which is seen to be true for both qG_p and G_{66} in Figs. 4 and 6), then at least one of others (*i.e.*, G_{44}, G_{55}, and/or qG_u) *must necessarily go up* at this stage of the calculation. Thus, we find that qG_u and G_{55} always go up with rotation angle, while shear modulus G_{44} has more complicated behavior depending also on the fracture density value. TABLE V shows explicitly how this works out in the trace and determinant values for the cases covered in our examples. The traces and determinants displayed here should be completely invariant (constant) as a function of rotation — except for the fact that these values are computed *after* the layer-averaging step, which causes some off-off-diagonal terms to average to zero. That they have a small (apparently random) deviation from perfect invariance provides a measure of the accuracy of our computational methods, for which it is believed that the largest numerical errors actually occur in the rotation step itself. Another test of the accuracy of the methods used is the fact that xthe Reuss and Voigt averages for the bulk modulus should both also remain invariant under these rotations [30]. This invariance (to numerical accuracy) is also demonstrated in Fig. 6, and provides another measure of the accuracy of the numerical procedures we used.

A fourth step in our analysis, which will be presented in the next section, is an attempt to estimate *via extrapolation* what happens at higher fracture densities, *i.e.*, beyond the region where the numerical results of Grechka and Kachanov [14] were available to help with quantification of the fracture influence parameters. This step uses a simple straight-line extrapolation method based on the best information currently available.

9. ESTIMATING FAILURE POINT VIA EXTRAPOLATION

One long-term goal of the work presented is to provide insight into modes of failure for fractured systems of the type considered. However, so far we have limited our discussion to fracture densities only up to $\rho = 0.2$, as this is the highest value considered in the numerical experiments of Grechka and Kachanov [14] that were subsequently used as the basis of the fitting techniques of Berryman and Grechka [13]. To do any more analysis, we need to come up with another approach.

One way to go beyond the available data would require extensive additional numerical modeling of the types discussed already. An alternative approach (but clearly one to be treated with special caution) is to develop an extrapolation method based on those numerical results already in hand. We present the results of such an extrapolation method in the present section of the paper.

9.1. Extrapolation technique

As already mentioned, a method of obtaining estimates beyond the range of our more certain knowledge is to use an extrapolation technique. One such approach would be to extrapolate simply by using the same expansion in powers of ρ that we have been using; but unfortuantely this approach will surely give misleading results, since it is clear that higher order fracture-influence coefficients (those multiplying higher powers of fracture density ρ) should come into play, and at the moment we have no way of knowing appropriate values for these purposes.

Another way of extrapolating is simply to extend the last line segment connecting certain values (say two of our fracture density values at $\rho = 0.1$ and 0.2) of the computed moduli to higher fracture density until the resulting line crosses zero (so the extrapolated modulus value is predicted to vanish approximaxtely at that fracture density by implication). Various effective moduli can be used for this purpose, including qG_p, G_{55}, G_{66}, and E_{33}, which are the smallest moduli and the ones that will clearly extrapolate to zero at the smallest values of ρ.

Using such an approach presumably does not give a very accurate value for the critical fracture density ρ_{crit}. However, since it is most likely that, as true critical values are approached, stronger fracture-fracture interactions will come into play (see [32, 33, 34]) — which have clearly been neglected here and which will necessarily cause the failure to happen even more quickly than our simple extrapolation procedure would predict. It seems plausible therefore that the extrapolated values obtained this way should prove to be reasonably reliable upper bounds on the true zero-modulus or failure point.

To summarize the details of the extrapolation method, consider M to be any modulus, and fit its changing value with ρ to a straight line according to:

$$M(\rho) = A + B\rho, \tag{13}$$

Then, if $M(\rho_1) = M_1$ and $M(\rho_2) = M_2$, it is not difficult to show that

$$A = \frac{\rho_2 M_1 - \rho_1 M_2}{\rho_2 - \rho_1} \quad \text{and} \quad B = -\frac{M_1 - M_2}{\rho_2 - \rho_1}. \tag{14}$$

The extrapolated value for the critical fracture density is therefore:

$$\rho_{crit} = -A/B. \tag{15}$$

Table IV. Extrapolated values of the critical crack density ρ_{crit} for failure (*i.e.*, being defined for present purposes as any elastic modulus M going to zero), using the procedure outlined in the main text. Values of various moduli at $\rho = 0.10$ and $= 0.20$ are extrapolated to zero for various angles (most often for angles of either 15° or 90°, and a few other examples for intermediate angles are also presented) between fractures in adjacent layers. Examples are listed in order of increasing values of their computed ρ_{crit}.

M	A	B	ρ_{crit}
$qG_p(90^o)$	2.231	-2.522	0.885
$E_{33}(45^o)$	5.101	-5.758	0.886
$G_{55}(15^o)$	2.228	-2.463	0.904
$E_{33}(60^o)$	5.601	-6.105	0.917
$G_{44}(15^o)$	2.215	-2.403	0.922
E_{22} & $E_{33}(90^o)$	6.041	-6.269	0.964
$E_{33}(30^o)$	5.201	-5.376	0.968
$E_{33}(15^o)$	5.130	-5.091	1.008
$qG_u(60^o)$	2.136	-2.095	1.020
K_R	9.967	-9.652	1.033
$G_{44}(45^o)$	2.133	-1.793	1.190
G_{55} & $G_{66}(90^o)$	2.231	-1.474	1.513
$G_{44}(90^o)$	2.037	-1.067	1.909

TABLE IV presents the results obtained by extrapolating the curves for qG_p, G_{44}, G_{55}, G_{66}, E_{33}, E_{22}, and K_R to zero according to the ideas just outlined. These results seem to give reasonable predictions, since the best (*i.e.*, lowest) extrapolated values are in the range $\rho_{crit} \simeq 0.8\text{-}1.0$. We view these numbers as likely upper bounds on the true critical fracture density. So the results are showing us that values in the range $\rho_{crit} \simeq 0.5 - 1.0$ are reasonable predictions, based on our extrapolations. These values are also consistent with the field results of Wu and Pollard [35] on the Fracture Spacing Index, among many others. The technical implications of this point are discussed more fully in the next subsection.

9.2. Comparisons to field observations

It turns out that the numerical estimates obtained using this procedure are nevertheless (perhaps surprisingly) consistent with field data on joint spacing in outcrops. Wu and Pollard [35] show that a typical relationship between joint spacing and layering thickness is given by

$$\alpha_i = D/T, \tag{16}$$

where D is mean joint spacing and T is bed thickness. The proportionality between the two is therefore the straight line (with zero intercept): $D = \alpha_i T$.

It is typically believed that these lines do not change with bed thickness, and that they are in fact functions of both lithology and mechanical properties. The so-called Fracture Spacing Index (FSI $\equiv 1/\alpha_i$) has been observed by these and other authors to lie typically in the range $0.1 \leq 1/\alpha_i \leq 0.5$, with some observed FSI values being as high as 1.3. Note that, in equation (7), we defined the crack density for flat and ribbon-shaped fractures to be $\rho_r = \pi h/4s \simeq h/s$, where h was height, and s was spacing of fractures. But, if we compare these definitions to

Table V. Trace $\mathbf{Tr}(\mathbf{S})$ and determinant $\mathbf{Det}(\mathbf{S})$ of the effective compliance matrix $\mathbf{S}$ (in the Kelvin form) for the layered system as a function of fracture density ρ and rotation angle Θ_F. This quantitative information provides a useful check on the matrix rotation processing step of the calculation.

ρ	Θ_F	$\mathbf{Tr}(\mathbf{S})$ (GPa^{-1})	$\mathbf{Det}(\mathbf{S})$ (GPa^{-6})
0.00	all	1.156127	1.1984×10^{-5}
0.05	15°	1.2129	2.130×10^{-5}
	30°	1.2128	2.144×10^{-5}
	45°	1.2128	2.129×10^{-5}
	60°	1.2130	2.174×10^{-5}
	90°	1.2128	2.128×10^{-5}
0.10	15°	1.2666	3.064×10^{-5}
	30°	1.2665	3.099×10^{-5}
	45°	1.2665	3.150×10^{-5}
	60°	1.2663	3.201×10^{-5}
	90°	1.2665	3.249×10^{-5}
0.20	15°	1.3662	4.809×10^{-5}
	30°	1.3665	4.842×10^{-5}
	45°	1.3662	4.965×10^{-5}
	60°	1.3661	5.099×10^{-5}
	90°	1.3668	5.382×10^{-5}

those of Wu and Pollard [35], we find that $h = T$ and $s = D$. So, except for the numerical factor $\pi/4$ of order unity, we have:

$$\rho_r \simeq FSI = 1/\alpha_i = T/D = h/s. \qquad (17)$$

We find therefore that the predictions of the relatively simple effective medium theory presented here is giving reasonable numbers for these fractured systems up to, but not all the way into, the complicated region of failure and rubblization. In particular, the methods employed have all been deterministic, and it is clear that important effects in geological, and other systems as well, involve randomness of fracture occurrence, orientation, and relative placement, none of which has been treated directly in the preceding analysis.

It is believed that the most appropriate view to take of these extrapolated values is that they are *likely* (though possibly quite crude) upper bounds on the true critical fracture density for failure of the systems studied. No more rigorous interpretation of these results is possible at the present time.

10. CONCLUSIONS

The method developed here uses some fairly standard methods from effective medium theories to treat complicated fracture systems and thus quantify their elastic behavior when fractures at moderately high densities are contiguous, but not intersecting. We find that one of the

weakest modes of the system studied is a quasi-pure shear mode that is an exact eigenmode of the constructed system, but not a true pure shear mode in the usual sense. TABLE IV shows these results. Other shear modes, including those correspoinding to shear moduli G_{44} and G_{55} at a rotation angle of about 15°, also lead to similar conclusions, and these modes are true torsional shear modes, as well as also being true eigenvalues of the system.

Results therefore indicate that the approach has some promise for enabling prediction of system failure (as a function of fracture density) and also prediction of which specific modes of failure are most likely to be active.

It may also be worth noting that, while we have phrased the problem here in terms of fractures in a field setting, the same ideas apply with equal validity to smaller scale systems such as laboratory scale rock deformation studies [36]. Indeed, the types of failure modes seen in the laboratory fall equally well within the general framework discussed here, and the analysis may prove useful for analyzing specific laboratory test data sets. Such directions for data analysis will provide a further motivation for future efforts along these, and similar related, lines of inquiry.

Finally, we have not yet discussed the influences that fluids in the fractures might have on the preceding analysis. Berryman [37] shows how Skempton's coefficient B [38, 39] may be used to introduce fluid effects simply into the Sayers and Kachanov [26] fractured systems analysis scheme that we also used here. This approach automatically makes the equations for fractured systems Gassmann consistent [37]. The mathematical approach presented here can be easily modified to account for these effects in the same way as in Ref. [37]. The main conclusion will follow that, due to the very slow changes inherent in the geological processes, these systems will typically (especially for rock outcrops) act as drained systems, and therefore will be largely unaffected mechanically by the presence of pore fluids. This story would change, however, if any liquid is trapped, so it is an undrained fluid with a significant bulk modulus (*i.e.*, a liquid). Such confined fluid would then tend to stiffen the system, and the corrections in [37] could be applied to account for these changes. We will say no more about these interesting effects here, as further elaboration of this story will need to be continued in another contribution.

APPENDIX A: SCHOENBERG-MUIR METHOD

The compliance form of the quasi-static equations of elasticity are typically written in the following way when the Voigt six-by-six matrix notation is being used:

$$
\begin{pmatrix} \epsilon_{11} \\ \epsilon_{22} \\ \epsilon_{33} \\ \epsilon_{23} \\ \epsilon_{31} \\ \epsilon_{12} \end{pmatrix} = \begin{pmatrix} S_{11} & S_{12} & S_{13} & S_{14} & S_{15} & S_{16} \\ S_{21} & S_{22} & S_{23} & S_{24} & S_{25} & S_{26} \\ S_{31} & S_{32} & S_{33} & S_{34} & S_{35} & S_{36} \\ S_{41} & S_{42} & S_{43} & S_{44} & S_{45} & S_{46} \\ S_{51} & S_{52} & S_{53} & S_{54} & S_{55} & S_{56} \\ S_{61} & S_{62} & S_{63} & S_{64} & S_{65} & S_{66} \end{pmatrix} \begin{pmatrix} \sigma_{11} \\ \sigma_{22} \\ \sigma_{33} \\ \sigma_{23} \\ \sigma_{31} \\ \sigma_{12} \end{pmatrix} \equiv \mathbf{S} \begin{pmatrix} \sigma_{11} \\ \sigma_{22} \\ \sigma_{33} \\ \sigma_{23} \\ \sigma_{31} \\ \sigma_{12} \end{pmatrix},
\tag{18}
$$

where $\mathbf{S}$ is the symmetric 6×6 compliance matrix. The numbers 1,2,3 always indicate Cartesian axes (say, x,y,z respectively). In many geological and geophysical applications, the 3-axis (or z-axis) is taken to be vertical, but we do *NOT* typically use this convention here. Instead, the z-direction is usually the layering direction, which can be oriented any direction in the earth. The principal stresses are σ_{11}, σ_{22}, σ_{33}, in the directions 1,2,3, respectively. Similarly, the principal strains are ϵ_{11}, ϵ_{22}, ϵ_{33}. The stresses σ_{23}, σ_{31}, σ_{12} are the called the torsional shear stresses, associated with rotation-based strains around the 1, 2, or 3 axes. Again, the corresponding torsional strains are ϵ_{23}, ϵ_{31}, and ϵ_{12}, where the torsional motion is a rotational straining motion around the 1, 2, or 3 axis, respectively. The compliance matrix is symmetric, so $S_{ij} = S_{ji}$, and this fact could have been used when writing out this matrix. However, there will be some advantages for our later analysis to leave the notation in this form for now. The axis pairs in the subscripts 11, 22, 33, 23, 31, and 12, are often labelled (following the conventions of Voigt [16, 17]) as 1,2,3,4,5,6, respectively. This choice of notation also clarifies the significance of the remaining pairs of subscripts appearing in the compliance matrix in (18).

The important contribution made by Backus [3] (also see Postma [40]) is the observation that, in a horizontally layered system, there are certain strains ϵ_{ij} and stresses σ_{ij} that are necessarily continuous across boundaries between layers, while the others are not necessarily continuous. We have been implicitly (and now explicitly by calling this fact out) assuming that the interfaces between layers are in welded contact, which means practically that the in-plane strains are always continuous: so if axis 3 (or z) is the symmetry axis (as is most often chosen for our layering problem), we have ϵ_{11}, $\epsilon_{12} = \epsilon_{21}$, and ϵ_{22} are all continuous. Similarly, in welded contact, we must have continuity of the all the stresses involving the 3 (or z) direction: so σ_{33}, $\sigma_{13} = \sigma_{31}$, and $\sigma_{23} = \sigma_{32}$ must all be continuous.

Then, following Backus [3] and/or Schoenberg and Muir [4], but now considering instead the compliance (inverse of stiffness) matrix, we have rearranged the statement of the problem so that:

$$
\begin{pmatrix} \epsilon_{11} \\ \epsilon_{22} \\ \epsilon_{12} \\ \epsilon_{33} \\ \epsilon_{32} \\ \epsilon_{31} \end{pmatrix} = \begin{pmatrix} S_{11} & S_{12} & S_{16} & S_{13} & S_{14} & S_{15} \\ S_{21} & S_{22} & S_{26} & S_{23} & S_{24} & S_{25} \\ S_{61} & S_{62} & S_{66} & S_{63} & S_{64} & S_{65} \\ S_{31} & S_{32} & S_{36} & S_{33} & S_{34} & S_{35} \\ S_{41} & S_{42} & S_{46} & S_{43} & S_{44} & S_{45} \\ S_{51} & S_{52} & S_{56} & S_{35} & S_{54} & S_{55} \end{pmatrix} \begin{pmatrix} \sigma_{11} \\ \sigma_{22} \\ \sigma_{12} \\ \sigma_{33} \\ \sigma_{32} \\ \sigma_{31} \end{pmatrix}.
\tag{19}
$$

Note that this equation, although similar to (18) is quite different because of the rearrangement of the matrix elements and the reordering of the strains and stresses. Expression of this equation can be made more compact by writing it as:

$$
\begin{pmatrix} X_T \\ X_N \end{pmatrix} = \begin{pmatrix} S_{TT} & S_{TN} \\ S_{NT} & S_{NN} \end{pmatrix} \begin{pmatrix} \Sigma_T \\ \Sigma_N \end{pmatrix},
\tag{20}
$$

where

$$
S_{TT} \equiv \begin{pmatrix} S_{11} & S_{12} & S_{16} \\ S_{21} & S_{22} & S_{26} \\ S_{61} & S_{62} & S_{66} \end{pmatrix},
\tag{21}
$$

$$S_{NN} \equiv \begin{pmatrix} S_{33} & S_{34} & S_{35} \\ S_{43} & S_{44} & S_{45} \\ S_{53} & S_{54} & S_{55} \end{pmatrix}, \tag{22}$$

and

$$S_{NT} \equiv \begin{pmatrix} S_{31} & S_{32} & S_{36} \\ S_{41} & S_{42} & S_{46} \\ S_{51} & S_{52} & S_{56} \end{pmatrix}, \tag{23}$$

with $S_{TN} = S_{NT}^T$ (with T superscript indicating the matrix transpose), and also where

$$X_T \equiv \begin{pmatrix} \epsilon_{11} \\ \epsilon_{22} \\ \epsilon_{12} \end{pmatrix}, \quad \text{and} \quad X_N \equiv \begin{pmatrix} \epsilon_{33} \\ \epsilon_{32} \\ \epsilon_{31} \end{pmatrix}, \tag{24}$$

and

$$\Sigma_T \equiv \begin{pmatrix} \sigma_{11} \\ \sigma_{22} \\ \sigma_{12} \end{pmatrix}, \quad \text{and} \quad \Sigma_N \equiv \begin{pmatrix} \sigma_{33} \\ \sigma_{32} \\ \sigma_{31} \end{pmatrix}. \tag{25}$$

It is most helpful to distinguish between "slow" and "fast" variables in this analysis, since this distinction makes it easy to decide when and how averaging should be performed. The "slow" variables, that are those continuous across the boundaries and also essentially constant for the present quasi-static application, are those contained in X_T and Σ_N. So, after averaging $\langle \cdot \rangle$ along the layering direction, we will have:

$$\begin{pmatrix} X_T \\ \langle X_N \rangle \end{pmatrix} = \begin{pmatrix} S_{TT}^* & S_{TN}^* \\ S_{NT}^* & S_{NN}^* \end{pmatrix} \begin{pmatrix} \langle \Sigma_T \rangle \\ \Sigma_N \end{pmatrix}, \tag{26}$$

where $S_{TN}^* = (S_{NT}^*)^T$, and all the starred quantities are the *nontrivial* average compliances we seek. They are defined in terms of layer average quantities where the symbol $\langle \cdot \rangle$ indicates a simple volume average of all the layers. By this we mean that a quantity Q that takes on different values in different layers has the layer average $\langle Q \rangle \equiv x_a Q_a + x_b Q_b + \dots$. The definition is general and applies to an arbitrary number of different layers where the fraction of the total volume occupied by layer a is x_a, etc. Total fractional volume is $x_a + x_b + \dots \equiv 1$. In our present application, we will treat only two types of layers, and each occupies half the volume, so $\langle Q \rangle = \frac{1}{2}(Q_a + Q_b)$. The method is however immediately generalized to an arbitrary number of different layers, and any relative weighting, when needed. Specific results presented here are however limited to the two-layer case.

Of the three final results, the ones easiest to compute are these two:

$$S_{TT}^* = \langle S_{TT}^{-1} \rangle^{-1}, \tag{27}$$

$$S_{TN}^* = (S_{NT}^*)^T = \langle S_{TT}^{-1} \rangle^{-1} \langle S_{TT}^{-1} S_{TN} \rangle = S_{TT}^* \langle S_{TT}^{-1} S_{TN} \rangle, \tag{28}$$

where $\langle \cdot \rangle$ is the layer average of some quantity. These results follow from this equation:

$$\langle S_{TT}^{-1} \rangle X_T = \langle \Sigma_T \rangle + \langle S_{TT}^{-1} S_{TN} \rangle \Sigma_N, \tag{29}$$

which followed immediately from the formula

$$X_T = S_{TT} \Sigma_T + S_{TN} \Sigma_N \tag{30}$$

multiplying through first by the inverse of S_{TT}, and then performing the layer average. [Note that S_{TT} and S_{NN} are both normally square and invertibxle matrices, whereas there will be many systems for which the off-diagonal matrix S_{NT} is not invertible. But, this fact is not an issue, because we do not need to invert S_{NT} in order to solve the averaging problem at hand.] These averages are meaningful because when the matrix equations presented are multiplied out, we never have any cross products of two quantities that are both unknown. [From this view point, Eq. (29) is an equation for $\langle \Sigma_T \rangle$, just as the unaveraged version of (29) is an equation for Σ_T in each layer.] So simple layer averaging

suffices (thereby providing the main motivation and value of this method). Multiplying (29) through by $\left\langle S_{TT}^{-1} \right\rangle^{-1}$ then gives the results (27) and (28).

The remaining result needed here requires more steps to compute, but the final result is given by:

$$S_{NN}^* = \langle S_{NN} \rangle - \left\langle S_{NT} S_{TT}^{-1} S_{TN} \right\rangle + S_{NT}^* \left(S_{TT}^* \right)^{-1} S_{TN}^*. \tag{31}$$

To provide some clues to the derivation, again consider:

$$\Sigma_T = S_{TT}^{-1} X_T - S_{TT}^{-1} S_{TN} \Sigma_N, \tag{32}$$

which is just a rearrangement of (30). The point is that $\langle \Sigma_T \rangle$ is then given immediately in terms of the quantities X_T and Σ_N, which are both "slow" variables and therefore essentially constant. An intermediate result that helps to explain the form of this relation (31) is:

$$S_{NT}^* \left(S_{TT}^* \right)^{-1} S_{TN}^* = \left\langle S_{NT} S_{TT}^{-1} \right\rangle \left\langle S_{TT}^{-1} \right\rangle^{-1} \left\langle S_{TT}^{-1} S_{TN} \right\rangle = \left\langle S_{NT} S_{TT}^{-1} \right\rangle S_{TN}^*. \tag{33}$$

Substituting for Σ_T from (32) into

$$X_N = S_{NT} \Sigma_T + S_{NN} \Sigma_N \tag{34}$$

and then averaging, we find that

$$\langle X_N \rangle = \left\langle S_{NT} S_{TT}^{-1} \right\rangle X_T + \left\langle S_{NN} - S_{NT} S_{TT}^{-1} S_{TN} \right\rangle \Sigma_N, \tag{35}$$

which completely determines all the remaining coefficients. After some more algebra, we find the formula determining the final result is actually given explicitly by:

$$\begin{aligned} \langle X_N \rangle \; &= \left\langle S_{NT} S_{TT}^{-1} \right\rangle \left\langle S_{TT}^{-1} \right\rangle^{-1} \left[\langle \Sigma_T \rangle + \left\langle S_{TT}^{-1} S_{TN} \right\rangle \Sigma_N \right] \\ &+ \left(\langle S_{NN} \rangle - \left\langle S_{NT} S_{TT}^{-1} S_{TN} \right\rangle \right) \Sigma_N \\ &= S_{NT}^* \langle \Sigma_T \rangle + S_{NN}^* \Sigma_N. \end{aligned} \tag{36}$$

Equation (36) contains all the information needed to produce the third and final result found in (31).

Another way to check these formulas is to compare them to those found in Schoenberg and Muir [4]. Direct comparison is not trivial; their analysis treats the stiffness version of the equations, while we are considering the compliance version here. Nevertheless, the symmetries of the equations are almost identical, so these useful comparisons and cross-checks will be left to the motivated reader.

APPENDIX B: BACKUS METHOD

The preceding Appendix A presented one method (that of Schoenberg and Muir [4]) for applying the general approach of Backus [3] to layer averaging in elasticity. Another method will be adopted in this Appendix B. The point of the second method is to make the details visible, and show in particular that the method does result in the appropriate stress/strain continuity relations at the layer boundaries. These details are suppressed in the preceding method, but — as will be shown explicitly here — the desired conditions are nevertheless being automatically satisfied.

The key idea that is used in the Backus method is to note that certain subsets of the elastic stress and strain variables are necessarily continuous across the layer interfaces, for if they were not continuous then the layers could not be considered to be in welded contact. If – as is commonly assumed – the layering direction is the z (or 3) direction, then welded contact implies continuity of the transverse strains $X_T^T = (\epsilon_{11}, \epsilon_{22}, \epsilon_{12})$ and also the longitudinal stresses $\Sigma_N^T = (\sigma_{33}, \sigma_{32}, \sigma_{31})$. This choice of layering direction is completely arbitrary, and (as we will show here) other choices of layering direction are also equally valid. This concept leads to the idea of "slow" and "fast" stresses and strains. For quasi-statics, "slow" implies constant, and "fast" implies varying from layer to layer. For seismic wave propagation (being the subject of Backus's original work), "slow" and "fast" have slightly different interpretations, because the applied stresses and strains are varying locally as the

seismic wave passes through the layered medium. We are treating only the quasi-static problem in this paper, but will nevertheless continue to use the fast/slow terminology. To emphasize the "slow" (or constant) character of certain sets of variables, we will put bars over the variables or vectors of variables as appropriate. Thus, the "slow"-ness of vectors just discussed above will be emphasized by using the notations: $\overline{X}_T^T$ and $\overline{\Sigma}_N^T$. The remaining variables without overbars, are all "fast" variables, and determine the desired quantities at the end of our calculations by performing the layer average, so, for example, X_N is a "fast" variable, but $\langle X_N \rangle$ is its layer average. The layer average itself has exactly the same meaning here as in Appendix A.

B.1 – Schoenberg-Muir revisited

To show quickly how this approach works, we can start from equation (20):

$$\left(\begin{array}{c} \overline{X}_T \\ X_N \end{array} \right) = \left(\begin{array}{cc} S_{TT} & S_{TN} \\ S_{NT} & S_{NN} \end{array} \right) \left(\begin{array}{c} \Sigma_T \\ \overline{\Sigma}_N \end{array} \right). \tag{37}$$

However, this time we will rearrange equation (37) in a different manner, so that the slow variables form a vector mutliplying a matrix that, when mutliplied by this vector, gives the corresponding vector of the fast variables:

$$\left(\begin{array}{c} \Sigma_T \\ X_N \end{array} \right) = \left(\begin{array}{cc} S_{TT}^{-1} & S_{TT}^{-1} S_{TN} \\ S_{NT} S_{TT}^{-1} & [S_{NT} S_{TT}^{-1} S_{TN} - S_{NN}] \end{array} \right) \left(\begin{array}{c} \overline{X}_T \\ -\overline{\Sigma}_N \end{array} \right). \tag{38}$$

We are not showing the algebra required to arrive at this equation, as it was already implicit in the work of the previous Appendix A.

One advantage of the Backus [3] method is that once we have our equation in the form shown in (38), the layer averaging step is conceptually trivial:

$$\left(\begin{array}{c} \langle \Sigma_T \rangle \\ \langle X_N \rangle \end{array} \right) = \left(\begin{array}{cc} \langle S_{TT}^{-1} \rangle & \langle S_{TT}^{-1} S_{TN} \rangle \\ \langle S_{NT} S_{TT}^{-1} \rangle & \langle S_{NT} S_{TT}^{-1} S_{TN} - S_{NN} \rangle \end{array} \right) \left(\begin{array}{c} \overline{X}_T \\ -\overline{\Sigma}_N \end{array} \right). \tag{39}$$

It is straightforward to check that these results for the effective coefficients are identical to the ones obtained using the original Schoenberg-Muir [4] approach. This is not at all surprising, but it is nevertheless useful in order to check that the boundary conditions are being applied consistently and correctly in both cases.

For simple elasticity problems, there is no particular advantage of one of these implementation methods over the other. However, for generalizations to more complex problems such as poroelasticity and thermoelasticity having additional stresses (such as pore pressure) and strain-related quantities such as the increment of fluid content (see Berryman [41]), and/or temperature variables and thermal expansion responses, the original method of Backus [3] continues to be straightforward for such applications and extensions.

B.2 – Averaging along the z-direction

Because the Schoenberg-Muir [4] approach is a top-down method, we do not see explicitly what is happening within the details. In particular, it is important to emphasize here that it is possible to construct our layered medium in more than one way from the same building blocks of fractured layers that we are describing here. To make this point more concretely, we will show now in some detail how to do the actual averaging in two orthogonal directions. We emphasize that the results are then for two distinct final composites. The first will have the structure as seen from a side view in Fig. 3. The second will have the structure as seen from a top-down view in Fig. 8. Both are perfectly valid applications of the methods considered, but Fig. 3 is probably the more interesting case for the geologically motivated problems of most interest to the authors at the present time.

Using the overline notation to designate the "slow" variables, we now explicitly treat the problem of layering as seen in Fig. 3, where the rotations of the fractures have been performed around the 1-

or x-axis. The compliance matrix has the form shown in (12) after the rotations of the fractures from the 12- or xy-plane. The general form is:

$$
\begin{pmatrix}
\overline{\epsilon}_{11} \\
\overline{\epsilon}_{22} \\
\epsilon_{33} \\
\epsilon_{23} \\
\epsilon_{31} \\
\overline{\epsilon}_{12}
\end{pmatrix}
=
\begin{pmatrix}
S_{11} & S_{12} & S_{13} & S_{14} & & \\
S_{12} & S_{22} & S_{23} & S_{24} & & \\
S_{13} & S_{23} & S_{33} & S_{34} & & \\
S_{14} & S_{24} & S_{34} & S_{44} & & \\
& & & & S_{55} & S_{56} \\
& & & & S_{56} & S_{66}
\end{pmatrix}
\begin{pmatrix}
\sigma_{11} \\
\sigma_{22} \\
\overline{\sigma}_{33} \\
\overline{\sigma}_{23} \\
\overline{\sigma}_{31} \\
\sigma_{12}
\end{pmatrix},
\tag{40}
$$

where blank entries in the matrix are zeroes.

To produce the desired result, we need to rearrange these equations so that the "fast" variables are on the left, the "slow" variables are on the far right. Then, the matrix is adjusted accordingly. The steps in this procedure are somewhat tedious, but otherwise straightforward. The final result is:

$$
\begin{pmatrix}
\sigma_{11} \\
\sigma_{22} \\
\epsilon_{33} \\
\epsilon_{23} \\
\epsilon_{31} \\
\sigma_{12}
\end{pmatrix}
=
\begin{pmatrix}
X_{11} & X_{12} & X_{13} & X_{14} & & \\
X_{12} & X_{22} & X_{23} & X_{24} & & \\
X_{13} & X_{23} & X_{33} & X_{34} & & \\
X_{14} & X_{24} & X_{34} & X_{44} & & \\
& & & & X_{55} & -S_{56}/S_{66} \\
& & & & -S_{56}/S_{66} & -1/S_{66}
\end{pmatrix}
\begin{pmatrix}
\overline{\epsilon}_{11} \\
\overline{\epsilon}_{22} \\
\overline{\sigma}_{33} \\
\overline{\sigma}_{23} \\
\overline{\sigma}_{31} \\
-\overline{\epsilon}_{12}
\end{pmatrix},
\tag{41}
$$

where D is the determinant

$$
D = S_{11}S_{22} - S_{12}^2,
\tag{42}
$$

of the 2×2 submatrix, and with the X-component definitions:

$$
\begin{pmatrix}
X_{11} & X_{12} \\
X_{12} & X_{22}
\end{pmatrix}
=
\tfrac{1}{D}
\begin{pmatrix}
S_{22} & -S_{12} \\
-S_{12} & S_{11}
\end{pmatrix}
\tag{43}
$$

$$
\begin{pmatrix}
X_{13} & X_{14} \\
X_{23} & X_{24}
\end{pmatrix}
=
-\tfrac{1}{D}
\begin{pmatrix}
S_{22} & -S_{12} \\
-S_{12} & S_{11}
\end{pmatrix}
\begin{pmatrix}
S_{13} & S_{14} \\
S_{23} & S_{24}
\end{pmatrix},
\tag{44}
$$

and

$$
\begin{pmatrix}
X_{33} & X_{34} \\
X_{34} & X_{44}
\end{pmatrix}
=
\begin{pmatrix}
S_{33} & S_{34} \\
S_{34} & S_{44}
\end{pmatrix}
-\tfrac{1}{D}
\begin{pmatrix}
S_{13} & S_{23} \\
S_{14} & S_{24}
\end{pmatrix}
\begin{pmatrix}
S_{22} & -S_{12} \\
-S_{12} & S_{11}
\end{pmatrix}
\begin{pmatrix}
S_{13} & S_{14} \\
S_{23} & S_{24}
\end{pmatrix}.
\tag{45}
$$

The final X-component needed is

$$
X_{55} = S_{55} - S_{56}^2/S_{66}.
\tag{46}
$$

Once we have the equations rewritten in the form (41), the final layer averaging step is immediate. All the displayed matrix coefficients can be averaged directly, and the results for the averaged stresses and strains in terms of the boundary interface quantities are easily found. For example, $\langle\epsilon_{33}\rangle = \langle X_{13}\rangle\overline{\epsilon}_{11} + \langle X_{23}\rangle\overline{\epsilon}_{22} + \langle X_{33}\rangle\overline{\sigma}_{33} + \langle X_{43}\rangle\overline{\sigma}_{23}$, gives the relationships between the averaged strain $\langle\epsilon_{33}\rangle$ (recall that the averaged strain/stress is also the macroscopic strain/stress in such a layered medium), and the boundary values of those stresses and strains are continuous across the layer boundaries. For this case, the averaging is along the z (or 3) direction. A similar calculation will be performed in the following subsection (B.3) for averaging along the x (or 1) direction. In general the averaging can be performed in any arbitrary direction, but, the farther this direction is from a symmetry axis of the elastic matrix (tensor), the fuller is the elastic matrix and the harder it is to write down the details explicitly, as is being done here.

One immediately useful observation about these coefficients is this: The coefficients S_{14}, S_{24}, S_{34}, and S_{56} are the only coefficients in the matrix of (40) that prevent the matrix symmetry from being orthorhombic. But these four possibly nonzero components off-off-diagonal coefficients have been shown to have opposite signs in the two layers we are considering for the averaging step of this calculation. Thus, $\langle S_{14}\rangle = \langle S_{24}\rangle = \langle S_{34}\rangle = \langle S_{56}\rangle \equiv 0$, after the indicated layer averaging. Since all
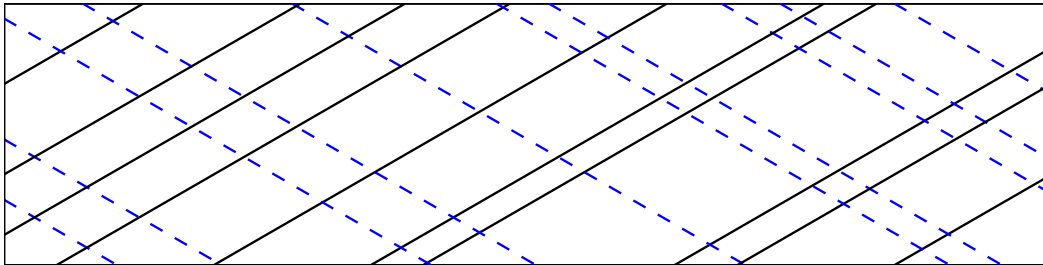
Figure 8. Example of a top view of another type of layered medium that can also be treated by the methods presented in the text. The layers are stacked top to bottom with only two types of these layers being shown. Individual layers are fractured/fractured, each having the same fracture density but not necessarily the same spatial distribution of fractures. For this example, the planes of the flat fractures shown are all at either $\pm 30^o$ from the planes of intersection. All fractures in a given layer have the same angular orientation. Solid lines are the fractures in the layer nearer to the viewer. The dashed lines (also in blue) are for the fractures in the hidden layer below the nearer layer. As in Fig. 5, all fractures are seen edge on.

the remaining elastic coefficients in the two layers are identical [*i.e.*, having $S_{12}^a = S_{12}^b$, etc.], then all averages must vanish when they have one of these three changeable coefficients either standing alone, or multiplying other coefficients that do not change sign between layers; thus, for example, $\langle S_{56}/S_{66} \rangle = \langle S_{56} \rangle /S_{66} = 0$. [Obviously, squares or cross-products of the coefficients having this symmetry property do NOT average to zero, but such terms appear mostly along the diagonal of the elastic matrix, and therefore do not affect our main arguments.] This observation shows that the final degree of symmetry of the layer-averaged system will not be any more complicated than orthorhombic. [A small amount of additional mathematics is required to prove this, but these details will be left as an exercise for the reader.] The authors had also tried the Schoenberg-Muir [4] version of the averaging scheme first, and discovered that this orthorhombic symmetry was in fact always obtained. But, unfortunately, the explanation for the behavior was not so obvious from this alternate point of view. The argument just given shows, in a relatively simple way, why this must always happen for the choices of layer symmetry that we have made here.

B.3 – Averaging along the x-direction

In this subsection, we repeat the calculations of the preceding subsection in order to illustrate how the results of the method can differ when the layering (and therefore averaging) direction is chosen along another orthogonal direction. The starting point is exactly the same as in the preceding subsection, namely Eq. (40), except that now the choices of continuous stresses and strains (as indicated by the overlines) is different:

$$
\begin{pmatrix} \epsilon_{11} \\ \overline{\epsilon}_{22} \\ \overline{\epsilon}_{33} \\ \overline{\epsilon}_{23} \\ \epsilon_{31} \\ \epsilon_{12} \end{pmatrix} = \begin{pmatrix} S_{11} & S_{12} & S_{13} & S_{14} & & \\ S_{12} & S_{22} & S_{23} & S_{24} & & \\ S_{13} & S_{23} & S_{33} & S_{34} & & \\ S_{14} & S_{24} & S_{34} & S_{44} & & \\ & & & & S_{55} & S_{56} \\ & & & & S_{56} & S_{66} \end{pmatrix} \begin{pmatrix} \overline{\sigma}_{11} \\ \sigma_{22} \\ \sigma_{33} \\ \sigma_{23} \\ \overline{\sigma}_{31} \\ \overline{\sigma}_{12} \end{pmatrix},
\tag{47}
$$

In this case, the lower 2×2 submatrix problem is already in the form we want, so we need only to deal with the upper 4×4 submatrix problem. Using the same types of manipulations displayed in the

previous subsection, we find:

$$
\begin{pmatrix}
\epsilon_{11} \\
\sigma_{22} \\
\sigma_{33} \\
\sigma_{23} \\
\epsilon_{31} \\
\epsilon_{12}
\end{pmatrix}
=
\begin{pmatrix}
Y_{11}-S_{11} & Y_{12} & Y_{13} & Y_{14} & & \\
Y_{12} & Z_{22} & Z_{23} & Z_{24} & & \\
Y_{13} & Z_{23} & Z_{33} & Z_{34} & & \\
Y_{14} & Z_{24} & Z_{34} & Z_{44} & & \\
& & & & S_{55} & S_{56} \\
& & & & S_{56} & S_{66}
\end{pmatrix}
\begin{pmatrix}
-\overline{\sigma}_{11} \\
\overline{\epsilon}_{22} \\
\overline{\epsilon}_{33} \\
\overline{\epsilon}_{23} \\
\overline{\sigma}_{31} \\
\overline{\sigma}_{12}
\end{pmatrix},
\tag{48}
$$

where

$$
\begin{pmatrix}
Z_{22} & Z_{23} & Z_{24} \\
Z_{23} & Z_{33} & Z_{34} \\
Z_{24} & Z_{34} & Z_{44}
\end{pmatrix}
\equiv
\begin{pmatrix}
S_{22} & S_{23} & S_{24} \\
S_{23} & S_{33} & S_{34} \\
S_{24} & S_{34} & S_{44}
\end{pmatrix}^{-1},
\tag{49}
$$

$$
\begin{pmatrix}
Y_{12} \\
Y_{13} \\
Y_{14}
\end{pmatrix}
=
\begin{pmatrix}
Z_{22} & Z_{23} & Z_{24} \\
Z_{23} & Z_{33} & Z_{34} \\
Z_{24} & Z_{34} & Z_{44}
\end{pmatrix}
\begin{pmatrix}
S_{12} \\
S_{13} \\
S_{14}
\end{pmatrix},
\tag{50}
$$

and

$$
Y_{11} \equiv
\begin{pmatrix} S_{12} & S_{13} & S_{14} \end{pmatrix}
\begin{pmatrix}
Y_{12} \\
Y_{13} \\
Y_{14}
\end{pmatrix}.
\tag{51}
$$

Finally, it is not difficult to show that the layer-averaged terms $\langle Y_{14} \rangle$, $\langle Z_{24} \rangle$, $\langle Z_{34} \rangle$, and $\langle S_{56} \rangle$ all vanish, for the same reasons as discussed in the previous subsection. So once again, the symmetry of the layer-averaged problem is generally no more complicated than orthorhombic for the types of problems under consideration.

Although the x-averaging method just presented may prove useful is some contexts, our main interest in this paper concerns the z-averaging method – as this is the one that most closely mimics the behavior of fracture patterns observed in the field (see Figs. 1 and 2). So examples of the application of formulas (48) through (51) will not be included among our examples at the present time.

APPENDIX C: INVERTING THE 6×6 ELASTIC MATRICES

The elastic matrices for compliance and stiffness have very particular forms that make them relatively easy to invert. This fact is useful since we need to move back and forth between the two forms in the analysis of this paper.

Let $\mathbf{A}$, $\mathbf{B}$, and $\mathbf{C}$ be three 3×3 matrices, where $\mathbf{A}$ and $\mathbf{C}$ are invertible and symmetric, while $\mathbf{B}$ is, usually, neither invertible nor symmetric. Then, if the matrix

$$
\begin{pmatrix}
\mathbf{A} & \mathbf{B} \\
\mathbf{B}^T & \mathbf{C}
\end{pmatrix}
\tag{52}
$$

is one of the 6×6 elastic matrices, either compliance or stiffness, and

$$
\begin{pmatrix}
\mathbf{X} & \mathbf{Y} \\
\mathbf{Y}^T & \mathbf{Z}
\end{pmatrix}
\tag{53}
$$

is the inverse of (52), then we have

$$
\begin{pmatrix}
\mathbf{AX}+\mathbf{BY}^T & \mathbf{AY}+\mathbf{BZ} \\
\mathbf{B}^T\mathbf{X}+\mathbf{CY}^T & \mathbf{B}^T\mathbf{Y}+\mathbf{CZ}
\end{pmatrix}
=
\begin{pmatrix}
\mathbf{I} & \mathbf{0} \\
\mathbf{0} & \mathbf{I}
\end{pmatrix}
\tag{54}
$$

where $\mathbf{I}$ is the 3×3 identity matrix, and $\mathbf{0}$ a 3×3 matrix of zeroes. Then, we make use of the facts that $\mathbf{A}$ and $\mathbf{C}$ are invertible matrices, while $\mathbf{B}$ is usually not invertible, to obtain:

$$
\mathbf{Y} = -\mathbf{A}^{-1}\mathbf{BZ}, \qquad \text{and} \qquad \mathbf{Y}^T = -\mathbf{C}^{-1}\mathbf{B}^T\mathbf{X},
\tag{55}
$$

and so we have

$$\mathbf{X} = \left[\mathbf{A} - \mathbf{B}\mathbf{C}^{-1}\mathbf{B}^{T} \right]^{-1}, \quad \text{and} \quad \mathbf{Z} = \left[\mathbf{C} - \mathbf{B}^{T}\mathbf{A}^{-1}\mathbf{B} \right]^{-1}. \tag{56}$$

If (52) is the stiffness matrix in Voigt form, then it can be translated easily into the Kelvin form [9,11] as:

$$\begin{pmatrix} \mathbf{A} & \sqrt{2}\mathbf{B} \\ \sqrt{2}\mathbf{B}^{T} & 2\mathbf{C} \end{pmatrix} \tag{57}$$

while the Kelvin form [9,11] of the compliance matrix is then

$$\begin{pmatrix} \mathbf{X} & \frac{1}{\sqrt{2}}\mathbf{Y} \\ \frac{1}{\sqrt{2}}\mathbf{Y}^{T} & \frac{1}{2}\mathbf{Z} \end{pmatrix}. \tag{58}$$

It is easy to see that these transformations result in the same inverse relationships as shown previously in (55) and (56).

APPENDIX D: NUMERICAL PROCEDURE FOR OBTAINING ELASTIC EIGENVALUES AND EIGENVECTORS

Because the compliance matrix is 6×6, no matter what the symmetry of this matrix happens to be, it will have exactly six eigenvalues. For the cases that are well-approximated as being orthorhombic considered here, three of these eigenvalues may be correctly identified as shear moduli associated with torsional (twisting) shear. The remaining three eigenvalues however may or may not have simple physical interpretations, as it is commonly recognized that these other three eigenvalues can involve coupling between pure shear and pure compression. One of these modes may genrrally be characterized as a quasi-compressional mode having an effective bulk modulus (really a multiple of its inverse since we are considering the compliance matrix here) value associated with it. The other two modes may be characterized as quasi-shear modes.

D.1 – Eigenvalues

If we suppose this 3×3 submatrix of the elastic matrix can be written as

$$\begin{pmatrix} \frac{1}{E_{11}} & S_{12} & S_{13} \\ S_{12} & \frac{1}{E_{22}} & S_{23} \\ S_{13} & S_{23} & \frac{1}{E_{33}} \end{pmatrix}, \tag{59}$$

where the matrix elements shown all have their standard meanings (although in the present context this is also assumed to be true for the effective behavior of the homogenized/averaged medium), then it is always possible to compute the Reuss averages [42] for an effective bulk modulus and also for one effective shear modulus using this matrix. These averages turn out to be rigorous lower bounds on the bulk and shear moduli (alternatively, the inverse results correspond to upper bounds on the bulk and shear compliances) for isotropic polycrystals composed of a jumble of such single crystals, and they are pertinent to the stresses σ_{11}, σ_{22}, and σ_{33}, and the strains ϵ_{11}, ϵ_{22}, and ϵ_{33} of such a composite mixture of locally orthorhombic constituents.

Of these Reuss averages, the one for the bulk modulus has the further advantage that, even though it is usually not an actual eigenvalue of the matrix, it is nevertheless truly the bulk modulus of the locally anisotropic constituents. To see that this is so, apply a constant hydrostatic stress (pressure if you like) to the system having $\sigma = \sigma_{11} = \sigma_{22} = \sigma_{33}$. Then, the volumetric strain is

$$\epsilon = \epsilon_{11} + \epsilon_{22} + \epsilon_{33} = \frac{\sigma}{K_R}, \tag{60}$$

where

$$\frac{1}{K_R} \equiv \frac{1}{E_{11}} + \frac{1}{E_{22}} + \frac{1}{E_{33}} + 2\left(S_{12} + S_{13} + S_{23}\right). \tag{61}$$

We see that this prescription clearly gives the correct value for the bulk modulus in the isotropic case, where $1/3K = (1-2\nu)/E$ and $S_{12} = S_{13} = S_{23} = -\nu/E$, with ν being Poisson's ratio. Our point is that a single crystal of any anisotropic elastic material has a meaningful bulk modulus that can be experimentally determined in exactly this way (*e.g.*, through immersion in a pressurized water bath).

One reason for stressing this point now is that we need to obtain three meaningful and easily interpretable constants from our computed anisotropic elastic tensor/matrix (59) as efficiently as possible. The eigenvalue equation for this 3×3 submatrix is cubic. Cubic equations with real coefficients can be solved analytically as described in standard references [43, 44], or it can also be solved starting with a Newton-Raphson iteration scheme [45] to find a single eigenvalue. The eigenvalue associated with the Reuss estimate of the bulk modulus is clearly a good choice for starting such a numerical iteration procedure. So, after iterating to convergence and having thus presumably found the eigenvalue most closely associated will compression and/or tension, we can subsequently deflate the cubic eigenvalue problem [45] to a quadratic equation, which can then be solved analytically with no further difficulty, using the very well-known quadratic formula.

The approach this works well as has been described previously in a different physical context by Berryman and Wang [46]. Our cubic polynomial equation is

$$P(x) = \sum_{n=0}^{3} P_n(-x)^n = (x_1 - x)(x_2 - x)(x_3 - x) = 0, \tag{62}$$

where $P_3 = 1$, $P_2 = (x_1 + x_2 + x_3)$, $P_1 = (x_1 x_2 + x_2 x_3 + x_3 x_1)$, and $P_0 = x_1 x_2 x_3$. And also we have from (59), the determinant

$$\det \begin{pmatrix} \frac{1}{E_{11}} - x & S_{12} & S_{13} \\ S_{12} & \frac{1}{E_{22}} - x & S_{23} \\ S_{13} & S_{23} & \frac{1}{E_{33}} - x \end{pmatrix} = 0, \tag{63}$$

which implies that

$$\begin{aligned}
P_0 &= \frac{1}{E_{11}E_{22}E_{33}} + 2S_{12}S_{23}S_{13} - \frac{S_{23}^2}{E_{11}} - \frac{S_{13}^2}{E_{22}} - \frac{S_{12}^2}{E_{33}}, \\
P_1 &= \frac{1}{E_{11}E_{22}} + \frac{1}{E_{22}E_{33}} + \frac{1}{E_{33}E_{11}} + S_{12}^2 + S_{23}^2 + S_{13}^2, \\
P_2 &= \frac{1}{E_{11}} + \frac{1}{E_{22}} + \frac{1}{E_{33}}, \\
P_3 &= 1.
\end{aligned} \tag{64}$$

Using the linear independence of the terms in powers of x in (62), we also have the following three equations showing that

$$x_1 = P_2 - x_2 - x_3 = \frac{P_1 - x_2 x_3}{x_2 + x_3} = \frac{P_0}{x_2 x_3}. \tag{65}$$

But, in this form, (65) is only useful if we have already found two of the three solutions.

Instead we shall start with a guess based on the Reuss average for the system bulk modulus (as already discussed here), and then iterate according to

$$X^{(i)} = X^{(i-1)} - P(X^{(i-1)})/P'(X^{(i-1)}), \qquad \text{for} \qquad i = 1, 2, \ldots, N_c, \tag{66}$$

where P' is the first derivative of the polynomial $P(x)$. Iteration continues until some choice of convergence criterion has been satisfied when $i = N_c$. Since we are proposing to start the iteration with $X^{(0)} = 1/3K_R$, which is a rigorous upper bound on the value sought, we expect this iteration to proceed smoothly to the right root. The result of this process is $x_1 \simeq X^{(N_c)}$, with a small numerical error based on our choice of convergence criterion.

Once such an approximation to the first root x_1 has been obtained, then the other two roots are found by deflation of the cubic to a quadratic equation. One formula for doing this is based on (65), and given by

$$x_{2,3} = \frac{1}{2}\left[(P_2 - x_1) \pm \sqrt{(P_2 - x_1)^2 - 4P_0/x_1}\right]. \tag{67}$$

This result follows from the observation that the desired quadratic formula has the form:

$$(x - x_2)(x - x_3) = x^2 - (x_2 + x_3)x + x_2 x_3 = 0, \tag{68}$$

while (65) shows that

$$(x_2 + x_3) = P_2 - x_1 \qquad \text{and} \qquad x_2 x_3 = \frac{P_0}{x_1}. \tag{69}$$

Equation (67) follows after substituting (69) into (68) and solving for x_2 and x_3. Thus, we find both the quasi-shear effective moduli simultaneously and consistently, based xon the previously computed value of compliance associated with the initial guess $1/3K_R$, which is expected to produce the compliance associated with quasi-compression/quasi-tension.

It is also possible to solve the cubic equation (62) semi-analytically using either the Cardan or the trigonometric solutions [43, 44]. However, the other method proposed here is actually easier to implement numerically. Both methods were used in this work, and found useful for purposes of cross-checking and code debugging.

D.2 – Eigenvectors

One technical point still remaining is how these three compliances (*i.e.*, the eigenvalues $\lambda = x_1$, x_2, and x_3) should be interpreted. While the diagonal components of the compliance $1/E_{11}$, $1/E_{22}$, and $1/E_{33}$ all have easy interpretations in terms of directionality, the three eigenvalues are more fundamental quantities, yet they also require further work before they can be precisely interpreted.

For a 3×3 system, the hardest step is finding the first eigenvalue. Then, as shown in the preceding subsection, the other two eigenvalues are easy to find. Similarly, once we have all three eigenvalues, the three corresponding eigenvectors are also very easy to compute. In general [46], if $\lambda = x_1, x_2$, or x_3, then an eigenvector associated with one of these λ values is proportional to:

$$\begin{pmatrix} \alpha \\ \beta \\ \gamma \end{pmatrix} = \begin{pmatrix} S_{12}S_{23} - S_{13}\left(\frac{1}{E_{22}} - \lambda\right) \\ S_{13}S_{12} - S_{23}\left(\frac{1}{E_{11}} - \lambda\right) \\ \left(\frac{1}{E_{11}} - \lambda\right)\left(\frac{1}{E_{22}} - \lambda\right) - S_{12}^2 \end{pmatrix}. \tag{70}$$

It is straightforward to verify that (70) is an eigenvector of (59) whenever λ is any one of the eigenvalues. The verification step for the first two entries (*i.e.*, a and b) is simple algebra. The third entry needs a bit of extra work to verify; this work involves the equation for the eigenvalues themselves, which can be rewritten as

$$S_{13}\left[S_{12}S_{23} - S_{13}(\frac{1}{E_{22}} - \lambda)\right] + S_{23}\left[S_{13}S_{12} - S_{23}(\frac{1}{E_{11}} - \lambda)\right]$$
$$+ \left(\frac{1}{E_{33}} - \lambda\right)\left[\left(\frac{1}{E_{11}} - \lambda\right)\left(\frac{1}{E_{22}} - \lambda\right) - S_{12}^2\right] = 0, \tag{71}$$

which is seen to be identical to the statements that

$$S_{13}\alpha + S_{23}\beta + \left(\frac{1}{E_{33}} - \lambda\right)\gamma = 0, \tag{72}$$

or, equivalently, that

$$S_{13}\alpha + S_{23}\beta + \frac{1}{E_{33}}\gamma = \lambda\gamma. \tag{73}$$

This step is the final one needed in the proof that vector $(\alpha, \beta, \gamma)^T$ is an eigenvector of (59), when the value of λ is chosen to be one of the three eigenvalues.

One caveat that is worthy of note concerns the special case when $S_{12} \equiv 0$, while simultaneously $E_{11} \equiv E_{22}$. Then, the analysis degenerates, and the proposed form of the eigenvector in (70) will produce all zeroes. This degeneracy of the proposed form also occurs in the other very special case of perfect isotropy. Neither of these special cases is expected to play any role in the systems of interest to us in this paper, but the reader should be aware of these potential pitfalls associated with the formulas if an attempt were made to apply them to systems other than the ones we are considering here.

Another special case (although not so special that it is not pertinent to the cases actually considered here) is when the axes are perfectly aligned with the symmetry axes of the elastic matrix, in which case the resulting compliance matrix can be diagonal. This means that all the off-diagonal values satisfy $S_{12} = S_{23} = S_{13} = 0$. The formulas (70) are again degenerate as written in this case, since they always give $\alpha = \beta = 0$ if the off-diagonal components vanish. But having a truly diagonal system makes life very simple for such calculations, as it is then quite obvious what eigenvector corresponds to each eigenvalue. So this issue will play no role in the following analysis.

Figure 6 shows the results we obtained for the quasi-bulk modulus and the quasi-shear moduli. In addition, we have also plotted the Reuss average of the bulk modulus K_R, defined by

$$\frac{1}{3K_R} = \frac{1}{3} \sum_{i,j=1,3} S_{ij}, \tag{74}$$

which is well-known *not* to be an eigenvalue either for orthorhombic elastic media. nstead K_R is a rigorous lower bound on the effective bulk modulus of any anisotropic elastic system [24]. Figure 6 shows in particular that the Reuss average K_R is indeed proportional to a lower bound on the computed quasi-bulk modulus of these systems, and furthermore that K_R is also approximately constant for fixed fracture density ρ.

REFERENCES

1. Bai T, Maerten L, Gross MR, Aydin A. Orthogonal cross joints: Do they imply a regional stress rotation? *Journal of Structural Geology* 2002; **24**:77–88.
2. Pollard DD, Aydin A. Progress in understanding jointing over the past one hundred years. *Geological Society of America Bulletin* 1988; **100**:1181–1204.
3. Backus GE. Long-wave elastic anisotropy produced by horizontal layering. *Journal of Geophysical Research* 1962; **67**:4427–4440.
4. Schoenberg M, Muir F. A calculus for finely layered anisotropic media. *Geophysics* 1989; **54**:581–589.
5. Bristow J. Microcracks, and the static and dynamic elastic constants of annealed and heavily cold-worked metals. *British Journal of Applied Physics* 1960; **11**:81–85.
6. Berryman JG. Elastic and transport properties in polycrystals of cracked grains: Cross-property relations and microstructure. *International Journal of Engineering Science* 2008; **46**:500–512.
7. Hashin Z, Shtrikman S. A variational approach to the theory of elastic behaviour of polycrystals. *Journal of the Mechanics and Physics of Solids* 1962; **10**:343–352.
8. Hashin Z, Shtrikman S. A variational approach to the elastic behaviour of multiphase materials. *Journal of the Mechanics and Physics Solids* 1963; **11**:127–140.
9. Budiansky B, O'Connell RJ. Elastic moduli of a cracked solid. *International Journal of Solids and Structures* 1976; **12**:81–97.
10. Kachanov M. Effective elastic properties of cracked solids: Critical review of some basic concepts. *Applied Mechanics Reviews* 1992; **45**:305–336.
11. Kachanov M. Elastic solids with many cracks and realted problems. *Advances in Applied Mechanics*, vol. 30, Hutchinson J, Wu T (eds.). Academic Press, 1993; 256–426.
12. Sevostianov I, Kachanov M. On the elastic compliances of irregularly shaped cracks. *International Journal of Fracture* 2002; **114**:245–257.
13. Berryman JG, Grechka V. Random polycrystals of grains containing cracks: Model of quasistatic elastic behavior for fractured systems. *Journal of Applied Physics* 2006; **100**:113 527.
14. Grechka V, Kachanov M. Effective elasticity of rocks with closely spaced and intersecting cracks. *Geophysics* 2006; **71**:D85–D91.

15. Grechka V. Comparison of the non-interaction and differential schemes in predicting the effective properties of fractured media. *International Journal of Fracture* 2007; **144**:181–188.
16. Saenger EH. Numerical methods to determine effective elastic properties. *International Journal of Engineering Science* 2007; **46**:598–605.
17. Kelvin L. Elements of a mathematical theory of elasticity. Part 1: On stresses and strains. *Philosophical Transactions of the Royal Society* 1856; **166**:481–498.
18. Den Hartog JP. *Advanced Strength of Materials*. McGraw-Hill Book Company: New York, 1952.
19. Mehrabadi MM, Cowin SC. Eigentensors of linear anisotropic elastic-materials. *Quarterly Journal of Mechanics and Applied Mathematics* 1990; **43**:15–41.
20. Lamb H. *Hydrodynamics*. Cambridge University Press: Cambridge, UK, 1932.
21. Thomsen L. *Understanding Seismic Anisotropy in Exploration and Exploitation*. Society of Exploration Geophysicists: Tulsa, OK, 2002.
22. Milton GW. *The Theory of Composites*. Cambridge University Press: Cambridge, 2002.
23. Voigt W. *Lehrbuch der Kristallphysik*. Teubner: Leipzig, 1928.
24. Nye JF. *Physical Properties of Crystals: Their Representation by Tensors and Matrices*. Oxford Science Publications: Oxford, UK, 1985.
25. Kachanov M. A continuum model of medium with cracks. *ASCE Journal of Engineering Mechanics* 1980; **106**:1039–1051.
26. Sayers CM, Kachanov M. A simple technique for finding effective elastic constants of cracked solids for arbitrary crack orientation statistics. *International Journal of Solids and Structures* 1991; **27**:671–680.
27. Sayers CM, Kachanov M. Microcrack-induced elastic-wave anisotropy of brittle rocks. *Journal of Geophysical Research – Solid Earth* 1995; **100**:4149–4156.
28. Dellinger J. Computing the optimal transversely isotropic approximation of a general elastic tensor. *Geophysics* 2005; **70**:I1–I10.
29. Berryman JG. Bounds and self-consistent estimates for elastic constants of random polycrystals with hexagonal, trigonal, and tetragonal symmetries. *Journal of the Mechanics and Physics of Solids* 2005; **53**:2141–2173.
30. Berryman JG. Bounds on elastic constants for random polycrystals of laminates. *Journal of Applied Physics* 2004; **96**:4281–4287.
31. Hill R. The elastic behaviour of crystalline aggregate. *Proceedings of the Physical Society of London* 1952; **A65**:349–354.
32. Toussaint R, Pride SR. Fracture of disordered solids in compression as a critical phenomenon. I. Statistical mechanics formalism. *Physical Review E* 2002; **66**:036 135.
33. Toussaint R, Pride SR. Fracture of disordered solids in compression as a critical phenomenon. II. Model Hamiltonian for a population of interacting cracks. *Physical Review E* 2002; **66**:036 136.
34. Toussaint R, Pride SR. Fracture of disordered solids in compression as a critical phenomenon. III. Analysis of the localization transition. *Physical Review E* 2002; **66**:036 137.
35. Wu H, Pollard DD. An experimental study of the relationship between joint spacing and layer thickness. *Journal of Structural Geology* 1995; **17**:887–905.
36. Paterson MS, Wong TF. *Experimental Rock Deformation – The Brittle Field*. Springer: New York, 2005.
37. Berryman JG. Seismic waves in rocks with fluids and fractures. *Geophysical Journal International* 2006; **171**:954–974.
38. Gassmann F. Über die Elastizität poröser Medien. *Vierteljahrsschrift der Naturforschenden Gesellschaft in Zürich* 1951; **96**:1–23.
39. Skempton AW. The pore-pressure coefficients *A* and *B*. *Geotechnique* 1954; **4**:143–147.
40. Postma GW. Wave propagation in a stratified medium. *Geophysics* 1955; **20**:780–806.
41. Berryman JG. Transversely isotropic poroelasticity arising from thin isotropic layers. *Mathematics of Multiscale Materials*, Golden KM, Grimmett GR, James RD, Milton GW, Sen PN (eds.). Springer: New York, 1998; 37–50.
42. Reuss A. Berechung der Fliessgrenze von Mischkristallen. *Z. Angew. Math. Mech.* 1929; **9**:49–58.
43. Abramowitz M, Stegun IA. *Handbook of Mathematical Functions*. Dover: New York, 1965.
44. Korn GA, Korn TM. *Mathematical Handbook for Scientists and Engineers: Definitioins, Theorems, and Formulas for Reference and Review*. Dover: Mineola, New York, 1968.
45. Press WH, Flannery BP, Teukolsky SA, Vetterling WT. *Numerical Recipes in C*. Cambridge University Press: Cambridge, UK, 1988.
46. Berryman JG, Wang HF. Elastic wave propagation and attenuation in a double-porosity dual-permeability medium. *International Journal of Rock Mechanics and Mining Sciences* 2000; **37**:63–78.